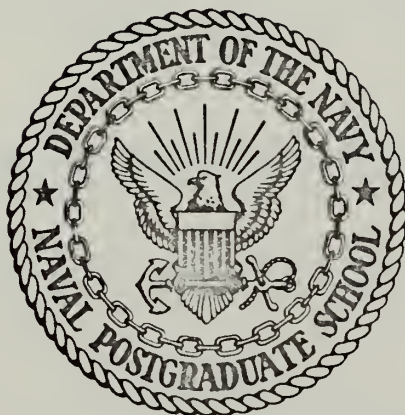


NUMERICAL SIMULATION OF THE
GENERATION OF GRAVITY WAVES IN A FRONTAL ZONE

Robert Ole Given

NAVAL POSTGRADUATE SCHOOL

Monterey, California



THESIS

Numerical Simulation
of the
Generation of Gravity Waves in a Frontal Zone

by

Robert Ole Given

Thesis Advisor:

Roger T. Williams

September 1972

T149504

Approved for public release; distribution unlimited.

Numerical Simulation
of the
Generation of Gravity Waves in a Frontal Zone

by

Robert Ole Given
Lieutenant Commander, United States Navy
B. B. A., State University of Iowa, 1963

Submitted in partial fulfillment of the
requirements for the degree of

MASTER OF SCIENCE IN METEOROLOGY

from the

NAVAL POSTGRADUATE SCHOOL
September 1972

Th 213
is 2573
10.1

ABSTRACT

The generation of gravity waves in a frontal zone is investigated with a numerical model. The solutions show that gravity waves can be generated in a frontal zone by the application of a heating function which varies sinusoidally with time, and that such waves propagate both ahead of and behind the frontal zone. The amplitude of the waves are directly proportional to the magnitude of the forcing function and to the period of sinusoidal oscillation. Even with large heating rates, no hydraulic jumps are formed.

TABLE OF CONTENTS

| | | |
|------|--------------------------------------|----|
| I. | INTRODUCTION..... | 8 |
| II. | BASIC EQUATIONS..... | 10 |
| III. | NUMERICAL PROCEDURES..... | 13 |
| IV. | NUMERICAL SOLUTIONS..... | 15 |
| V. | CONCLUSIONS AND RECOMMENDATIONS..... | 42 |
| | LIST OF REFERENCES..... | 44 |
| | INITIAL DISTRIBUTION LIST..... | 45 |
| | FORM DD 1473..... | 48 |

TABLE

TABLE

| | | |
|---|------------------------------|----|
| I | VARIATION OF PARAMETERS..... | 16 |
|---|------------------------------|----|

LIST OF ILLUSTRATIONS

| FIGURE | | PAGE |
|--------|--|------|
| 1a | Vertical velocity w maxima and the position of the front (---). Run number 1..... | 18 |
| 1b | Departure potential temperature θ' at level $z=1.5$ km. Run number 1..... | 18 |
| 2a | Divergent part of the wind v as a function of time at four levels: $z=.5$ km (1), $z=2.5$ km (3), $z=5.5$ km (6) and $z=8.5$ km (9). Run number 1..... | 19 |
| 2b | Divergent part of the wind v as a function of time at four levels: $z=.5$ km (1), $z=2.5$ km (3), $z=5.5$ km (6) and $z=8.5$ km (9). Run number 1..... | 20 |
| 3a | Departure potential temperature θ' as a function of time at four levels: $z=.5$ km (1), $z=2.5$ km (3), $z=5.5$ km (6) and $z=8.5$ km (9). Runs number 1 and 3..... | 21 |
| 3b | Departure potential temperature θ' as a function of time at four levels: $z=.5$ km (1), $z=2.5$ km (3), $z=5.5$ km (6) and $z=8.5$ km (9). Runs number 1 and 3..... | 22 |
| 4a | Vertical velocity w maxima and the position of the front (---). Run number 4..... | 24 |
| 4b | Departure potential temperature θ' at level $z=1.5$ km. Run number 4..... | 24 |
| 5a | Vertical velocity w maxima and the position of the front (---). Run number 6..... | 26 |
| 5b | Departure potential temperature θ' at level $z=1.5$ km. Run number 6..... | 26 |
| 6 | Departure potential temperature θ' as a function of time at four levels: $z=.5$ km (1), $z=2.5$ km (3), $z=5.5$ km (6) and $z=8.5$ km (9). Runs number 6, 12 mod, and 12..... | 27 |
| 7a | Vertical velocity w maxima and the position of the front (---). Run number 9..... | 28 |
| 7b | Departure potential temperature θ' at level $z=1.5$ km. Run number 9..... | 28 |
| 8a | Vertical velocity w maxima and the position of the front (---). Run number 10..... | 30 |
| 8b | Departure potential temperature θ' at level $z=1.5$ km. Run number 10..... | 30 |

| | | |
|-----|--|----|
| 9a | Vertical velocity w maxima and the position of the front (---). Run number 13..... | 31 |
| 9b | Departure potential temperature Θ' at level $z=1.5$ km. Run number 13..... | 31 |
| 10 | Departure potential temperature Θ' as a function of time at four levels: $z=.5$ km (1), $z=2.5$ km (3), $z=5.5$ km (6) and $z=8.5$ km (9). Run number 13..... | 32 |
| 11a | Vertical velocity w maxima and the position of the front (---). Run number 14..... | 34 |
| 11b | Departure potential temperature Θ' at level $z=1.5$ km. Run number 14..... | 34 |
| 12a | Divergent part of the wind v as a function of time at four levels: $z=.5$ km (1), $z=2.5$ km (3), $z=5.5$ km (6) and $z=8.5$ km (9). Run number 14..... | 35 |
| 12b | Divergent part of the wind v as a function of time at four levels $z=.5$ km (1), $z=2.5$ km (3), $z=5.5$ km (6) and $z=8.5$ km (9). Run number 14..... | 36 |
| 13 | Departure potential temperature Θ' as a function of time at four levels: $z=.5$ km (1), $z=2.5$ km (3), $z=5.5$ km (6) and $z=8.5$ km (9). Run number 14..... | 37 |
| 14a | Vertical velocity w maxima and the position of the front (---). Run number 15..... | 38 |
| 14b | Departure potential temperature Θ' at level $z=1.5$ km. Run number 15..... | 38 |
| 15 | Departure potential temperature Θ' as a function of time at four levels: $z=.5$ km (1), $z=2.5$ km (3), $z=5.5$ km (6) and $z=8.5$ km (9). Run number 15..... | 39 |

ACKNOWLEDGEMENTS

The author wishes to express his appreciation to Dr. Roger Terry Williams for his technical assistance, recommendations, encouragement, and for the use of his basic frontogenesis model which was modified for the experiments conducted.

Thanks are also expressed to Dr. Ronnie L. Alberty who served as second reader and provided information on the characteristics of severe storms.

The author, furthermore, wishes to thank the W. R. Church Computer Center at the Naval Postgraduate School on whose computer system IBM 360/67 all computations were performed.

A final acknowledgement is given to Susan R. Given who endured the author's exponentially decreasing level of patience and understanding while occupied with this thesis.

I. INTRODUCTION

Meteorologists involved in numerical weather prediction have for some time been filtering gravity waves out of their prediction models. This has been done because high frequency inertial-gravity oscillations could be generated which would give unrealistic pressure changes, obscuring the meteorological forecasts. Gravity waves may be meteorologically significant however in explaining irregularities in the ionosphere, and in some mesoscale phenomenon in the troposphere. Hines (1960) has suggested that internal atmospheric gravity waves may account for many of the irregularities observed in the lower ionosphere and that these waves may have their origin in the large energy regions of the lower troposphere. Gossard, Jensen and Richter (1971) have studied gravity waves of small amplitude with a high-resolution FM/CW radar sounder. Breeding (1972) investigated the creation of unstable regions in the atmosphere by internal gravity waves. Gossard (1962) has listed the following three mechanisms for generating internal waves in the troposphere:

"1. Internal waves can be generated as standing waves in the lee of topographic features.

"2. Gravity waves are often caused by a traveling boundary between two types of air of different density. This type of tropospheric wave train is short, lasting less than two hours. It is a fair-weather phenomenon, rarely associated with storm fronts.

"3. Oscillations which last for many hours are generally associated with tropospheric storms and synoptic scale features. These oscillations of long duration are usually generated by storms and frontal disturbances but the presence of a stable layer in the lower atmosphere is required."

Tepper (1952) postulated that gravity waves may be generated in the vicinity of a moving frontal zone if the zone moves into an area where a stable layer exists. As the waves move out they steepen into hydraulic jumps. He felt that large vertical motions caused by the jumps could lead to severe weather such as is found near squall lines. Kurth (1971) studied hydraulic jumps in a rotating, continuously stratified atmosphere. Numerical simulation of squall line formation was carried out by Sasaki (1959) and Ogura and Charney (1962). One of the objectives of the present study was to determine if such effects could occur near a properly simulated frontal zone.

Since the advent of satellite pictures and the technique of producing film loops showing "weather-in-motion" it has become evident that high speed gravity waves move out from the face of frontal zones (Fujita and Bohan, 1967).

In this study, the non-geostrophic frontogenesis model of Williams (1972a) is modified in an attempt to generate gravity waves in a frontal zone.

In section II, the Boussinesq equations are given and the modeling relations are introduced. In the model the time-dependent quantities are functions of y and z only. The basic wind deformation field is independent of time and height. The numerical procedures, boundary conditions and initial conditions are given in section III. Numerical results are presented and discussed in section IV. Conclusions and recommendations for further investigations are given in section V.

II. BASIC EQUATIONS

In this experiment the Boussinesq equations are employed and the domain is bounded by two rigid horizontal planes. The compressibility of the atmosphere, which is neglected in the Boussinesq approximation, should not be of qualitative importance since the density scale height in the atmosphere is much larger than the thickness of typical frontal zones. The replacement of the tropopause by a rigid horizontal surface will induce large errors in this region and prevents gravity waves from propagating out of the troposphere, but the resulting errors near the lower boundary should be small. Basic equation development follows the work of Williams (1972a).

The hydrostatic Boussinesq equations can be written in the following form when the earth's rotation and horizontal eddy viscosity are included,

$$\frac{\partial}{\partial t} V + \nabla \cdot (VV) + \frac{\partial}{\partial z} (wV) + \nabla \phi + f k \times V = A_m \nabla^2 V, \quad (\text{II.1})$$

$$\frac{\partial \theta}{\partial t} + \nabla \cdot (\theta V) + \frac{\partial (w\theta)}{\partial z} = A_\theta \nabla^2 \theta + Q, \quad (\text{II.2})$$

$$\nabla \cdot V + \frac{\partial w}{\partial z} = 0, \quad (\text{II.3})$$

$$\frac{\partial \theta}{\partial z} = g\theta/\theta_0, \quad (\text{II.4})$$

where θ_0 is a constant reference potential temperature; p_0 a constant reference pressure, $k = R/(C_p)$; $\theta = T(p_0/p)^k - \theta_0$, the departure of the potential temperature from θ_0 , $\phi = C_p \theta_0 (p/p_0)^k + gz$, the pressure function, $A_m \nabla^2 V$, the horizontal diffusion of momentum, $A_\theta \nabla^2 \theta$, the horizontal diffusion of heat, and Q the heating function.

An exact steady solution to this set of equations is given by

$$\left. \begin{aligned} V &= D (xi-yj) \\ w &= 0 \\ \phi &= \Phi \equiv \left[-D^2 (x^2 + y^2) / 2 \right] - f Dxy \\ \Theta &= 0 \end{aligned} \right\} , \quad (II.5)$$

where D is a constant. Cartesian coordinates have been introduced and f is taken to be constant. The horizontal velocity is a field of pure deformation and this deformation is given by 2D.

If departures from the fields (II.5) are independent of x, then they will remain independent of x. Thus, the dependent variables are subdivided as follows:

$$\left. \begin{aligned} V &= \left[D x + u(y, z, t) \right] i + \left[-Dy + v(y, z, t) \right] j \\ w &= w(y, z, t) \\ \Theta &= \Theta(y, z, t) \\ \phi &= \Phi(x, y) + \pi(y, z, t) \end{aligned} \right\} . \quad (II.6)$$

If these expressions are substituted into Eqs. (II.1)-(II.4), they become:

$$\frac{\partial u}{\partial t} + \frac{\partial (vu)}{\partial y} + \frac{\partial (wu)}{\partial z} - \frac{\partial V}{\partial y} u + V \frac{\partial u}{\partial y} - f v = A_m \frac{\partial^2 u}{\partial y^2} , \quad (II.7)$$

$$\frac{\partial v}{\partial t} + \frac{\partial (vv)}{\partial y} + \frac{\partial (wv)}{\partial z} + \frac{\partial}{\partial y} (vV) + \frac{\partial \pi}{\partial y} + f u = A_m \frac{\partial^2 v}{\partial y^2} , \quad (II.8)$$

$$\frac{\partial \Theta}{\partial t} + \frac{\partial (v\Theta)}{\partial y} + \frac{\partial (w\Theta)}{\partial z} + V \frac{\partial \Theta}{\partial y} = A_\theta \frac{\partial^2 \Theta}{\partial y^2} + Q , \quad (II.9)$$

$$\frac{\partial v}{\partial y} + \frac{\partial w}{\partial z} = 0 , \quad (II.10)$$

$$\frac{\partial \pi}{\partial z} = \frac{g \Theta}{\Theta_0} , \quad (II.11)$$

where $V = -Dy$. The boundary conditions are

$$w = 0, \quad z = 0, H , \quad (II.12)$$

where H is the distance between the horizontal plates.

If the vertical average of a quantity is defined as

$$\langle () \rangle \equiv \frac{1}{H} \int_0^H () dz ,$$

and the hydrostatic equation (II.11) is integrated with respect to z

and the vertical mean is removed, then

$$\pi - \langle \pi \rangle = \frac{g}{\theta_0} \left[\int_0^z \Theta dz - \left\langle \int_0^z \Theta dz \right\rangle \right] \quad . \quad (\text{II.13})$$

The y equation of motion may now be written in terms of $\pi - \langle \pi \rangle$.

If the vertical average of (II.10) and the boundary conditions (II.12) are used, then

$$\frac{\partial}{\partial y} \langle v \rangle = 0 \quad .$$

This equation states that the total disturbance y mass flux is independent of y . If the other variables have proper symmetry it follows that $\langle v \rangle$ must be an odd function of y which leads to

$$\langle v \rangle = 0 \quad . \quad (\text{II.14})$$

If the vertical average of (II.8) is taken, and (II.12) and (II.14) are used, then

$$\frac{\partial \langle vv \rangle}{\partial y} + \frac{\partial \langle \pi \rangle}{\partial y} + f \langle u \rangle = 0 \quad . \quad (\text{II.15})$$

This result is subtracted from (II.8) which yields

$$\begin{aligned} \frac{\partial}{\partial t} v + \frac{\partial}{\partial y} (vv - \langle vv \rangle) + \frac{\partial}{\partial z} (wv) + \frac{\partial}{\partial y} (vV) + \frac{\partial}{\partial y} (\pi - \langle \pi \rangle) \\ + f(u - \langle u \rangle) = A_m \frac{\partial^2 v}{\partial y^2} \end{aligned} \quad (\text{II.16})$$

Eqs. (II.7), (II.9), (II.10), (II.13) and (II.16) form a complete set which can be solved by a pure marching process.

III. NUMERICAL PROCEDURE

The arrangement of variables and the finite difference approximations are the same as those used by Williams (1967). In order to close the problem computational boundaries must be introduced in y . Since the disturbance velocity should die out at a sufficient distance from the axis of dilatation, then

$$v(\pm Y, z, t) = 0 \quad . \quad (III.1)$$

However, there is appreciable inflow across these computational boundaries since $V(\pm Y) = \pm DY$. The quantities u and θ which are advected across the boundaries must be specified independent of the interior values if computational stability is to be maintained (Platzman, 1954). Thus, the following boundary conditions are used:

$$\left. \begin{aligned} u[\pm(Y+\Delta y/2, z, t)] &= u[\pm(Y+\Delta y/2), z, 0] \\ \theta[\pm(Y+\Delta y/2, z, t)] &= \theta[\pm(Y+\Delta y/2), z, \theta] \end{aligned} \right\} . \quad (III.2)$$

The computational boundaries $y = \pm Y$ are placed between grid points so that the above conditions are actually applied at $y = \pm(Y+\Delta y/2)$. These conditions are replaced by time specified functions in some experiments.

These boundary conditions developed a weak nonlinear instability near the boundaries but this was removed by introducing a forward step every 72 time steps.

The initial temperature field, from Williams (1972a), is given by

$$\theta(y, z, 0) = (\partial \bar{\theta}_x / \partial z)(z - H/2) - A(2/\pi) \arctan(\sinh \alpha y), \quad (III.3)$$

were $\alpha = f \pi H^{-1} (g \theta_0^{-1} \partial \bar{\theta}_x / \partial z)^{-\frac{1}{2}}$. The quantity $\partial \bar{\theta}_x / \partial z$, which is constant, is the initial stability and A is one-half the total horizontal temperature variation. The initial x component of the velocity is given by

$$u(y, z, 0) = \frac{2}{\pi} \frac{g A \alpha}{f \theta_0} (z - H/2) \operatorname{sech}(\alpha y). \quad (\text{III.4})$$

The initial v field is obtained from the quasigeostrophic equation.

IV. NUMERICAL SOLUTIONS

The finite-difference forms of Eqs. (II.7), (II.9), (II.10), (II.13) and (II.16) are solved by a pure marching process. Experiments are conducted by varying boundary conditions and heating functions. The Williams model is allowed to run for four days by which time a frontal zone has stabilized as described by Williams (1972b). At four days, boundary conditions are changed or heating is introduced and the model runs for an additional four days. The parameters which describe the various experiments are given in Table I.

The procedure for initializing the heating function Q is as follows: At the end of four days, the vertical velocity field is scanned at $z=2.5$ km (level three) to determine the area of maximum vertical velocity, which corresponds to the leading edge of the frontal zone. A region R is defined which is the region where the heating function is applied. This region varies in width and vertical extent depending on the experiment. The function is applied as follows:

$$\begin{aligned} Q &= C g(t) G(y,z) \text{ in region } R, \\ Q &= 0 \text{ elsewhere.} \end{aligned}$$

Here C is the maximum heating added and $g(t)$ takes the value 1.0, or the following sinusoidal variation

$$g(t) = s \sin(\omega t)$$

where ω is the frequency. The function $G(y,z)$ takes either the value 1.0 for block heating or the value determined by the sine squared function

$$G(y,z) = s \sin^2 \left\{ \frac{\pi [y - y_0(z)]}{\text{width of heating zone}} \right\}$$

In later experiments, a cooling function is applied to the upper levels of the model to simulate evaporation. This cooling is only activated

| Run number | ΔY (10's of meters) | | Model width (+100's of km) | | ΔZ (km) | | Time step (100's of seconds) | | A_m, A (1000's of $m^2 \text{ sec}^{-1}$) | | C ($^{\circ}\text{K day}^{-1}$) in region R | | G (y,z) | | g (t) | | $2\pi/\omega$ (1000's) | | Levels where heating added | | Cooling above region R | | Maximum vertical velocity w (cm sec^{-1}) F: Occurs in the frontal zone. D: Displaced away from the frontal zone. | | No stable layer | Stable layer ahead of front only | Stable layer throughout the model | Strong stable layer throughout the model |
|------------|-----------------------------|----|----------------------------|---|-----------------|-----|------------------------------|-----------------|--|------|---|--|-----------|--|---------|--|------------------------|--|----------------------------|--|------------------------|--|--|---|-----------------|----------------------------------|-----------------------------------|--|
| 1 | 6 | 18 | 1 | 6 | 20 | 0 | | | | | | | | | | | | | | | | | 1.58F | ✓ | | | | |
| 2 | 6 | 18 | 1 | 6 | 20 | 0 | | | | | | | | | | | | | | | | | .98F | | ✓ | | | |
| 3 | 6 | 18 | 1 | 6 | 20 | 0 | | | | | | | | | | | | | | | | | 1.83F | | | ✓ | | |
| 4 | 6 | 18 | 1 | 6 | 20 | 10 | 1 | 1 | | 1-5 | | | | | | | | | | | | | 4.53F | | | ✓ | | |
| 5 | 6 | 18 | 1 | 6 | 20 | 10 | \sin^2 | 1 | | 1-5 | | | | | | | | | | | | | 4.03F | | | ✓ | | |
| 6 | 6 | 18 | 1 | 6 | 20 | 10 | \sin^2 | $\sin \omega t$ | 36 | 1-5 | | | | | | | | | | | | | 4.83D | | | ✓ | | |
| 7 | 6 | 18 | 1 | 6 | 20 | 3 | \sin^2 | $\sin \omega t$ | 36 | 3-7 | | | | | | | | | | | | | 1.91F | | | ✓ | | |
| 8 | 6 | 18 | 1 | 6 | 20 | 30 | \sin^2 | $\sin \omega t$ | 36 | 3-7 | | | | | | | | | | | | | 13.68D | | | ✓ | | |
| 9 | 6 | 18 | 1 | 6 | 20 | 50 | \sin^2 | $\sin \omega t$ | 36 | 1-5 | | | | | | | | | | | | | 21.04D | | | ✓ | | |
| 10 | 6 | 18 | 1 | 6 | 7 | 50 | \sin^2 | $\sin \omega t$ | 36 | 1-5 | | | | | | | | | | | | | 31.53D | | | ✓ | | |
| 11 | 6 | 18 | 1 | 6 | 20 | 30 | \sin^2 | $\sin \omega t$ | 36 | 3-7 | | | | | | | | | | | | | 15.07D | ✓ | | | | |
| 12 | 6 | 18 | 1 | 6 | 20 | 30 | \sin^2 | $\sin \omega t$ | 36 | 3-7 | ✓ | | | | | | | | | | | | 13.30D | | | | ✓ | |
| 13 | 6 | 18 | 1 | 6 | 20 | 30 | \sin^2 | $\sin \omega t$ | 36 | 3-7 | ✓ | | | | | | | | | | | | 13.12D | | ✓ | | | |
| 14 | 6 | 18 | 1 | 6 | 20 | 30 | \sin^2 | $\sin \omega t$ | 36 | 3-7 | ✓ | | | | | | | | | | | | 13.68D | | | ✓ | | |
| 15 | 6 | 18 | 1 | 6 | 20 | 30 | \sin^2 | $\sin \omega t$ | 52 | 3-7 | ✓ | | | | | | | | | | | | 18.27D | | | ✓ | | |
| 16 | 6 | 18 | 1 | 6 | 20 | 30 | \sin^2 | $\sin \omega t$ | 20 | 3-7 | ✓ | | | | | | | | | | | | 3.20F | | | ✓ | | |
| 17 | 3 | 27 | .33 | 3 | 20 | 30 | \sin^2 | $\sin \omega t$ | 36 | 8-20 | ✓ | | | | | | | | | | | | 7.69D | | | ✓ | | |
| 18 | 3 | 27 | 1 | 3 | 7 | 30 | \sin^2 | $\sin \omega t$ | 36 | 3-7 | ✓ | | | | | | | | | | | | 28.46D | | | ✓ | | |
| 19 | 3 | 27 | 1 | 3 | 7 | 3 | \sin^2 | $\sin \omega t$ | 36 | 3-7 | ✓ | | | | | | | | | | | | 3.17F | | | ✓ | | |
| 20 | 3 | 27 | 1 | 2 | 7 | 100 | \sin^2 | $\sin \omega t$ | 36 | 3-7 | ✓ | | | | | | | | | | | | 76.67D | | | ✓ | | |

TABLE I. Variation of parameters

when there is heating and it is zero otherwise. The magnitude of the cooling is equal to 20% of the heating below.

Run number one is a control run with no variation of parameters. Maximum vertical velocity and the approximate position of the frontal zone is shown in Fig. 1a. Departure potential temperature, which is $\theta' = \theta - \bar{\theta}_x$ where $\partial \bar{\theta}_x / \partial z$ is the initial stability, is shown in Fig. 1b. The divergent part of the wind at four y grid points is shown in Fig. 2a and Fig. 2b. Fig. 3a and Fig. 3b show the variation in the departure potential temperature in the control run and the same quantity in run number three where a stable layer is introduced at the beginning. In both cases, all waves are virtually damped out at the end of eight days.

Run number two tests Tepper's hypothesis that gravity waves will be generated if a frontal zone moves into an area where a stable layer exists. A stable layer is introduced at the end of four days ahead of the frontal zone at the -Y boundary between $z=1.5$ km and $z=2.5$ km where $\partial \bar{\theta}_x / \partial z$ was set equal to 8°K km^{-1} . No gravity waves or jump zones were noted.

Run number three is the same as the control run except for the introduction of a stable layer at both the $\pm Y$ boundaries at the beginning of the program. As in run number two, the layer is inserted between $z=1.5$ km and $z=2.5$ km and $\partial \bar{\theta}_x / \partial z$ is set equal to 8°K km^{-1} between these two levels. By the end of four days this stable layer had propagated throughout the model between levels $z=1.5$ km and $z=2.5$ km. The presence of a stable layer throughout the model did not appear to generate gravity waves or create jump zones.

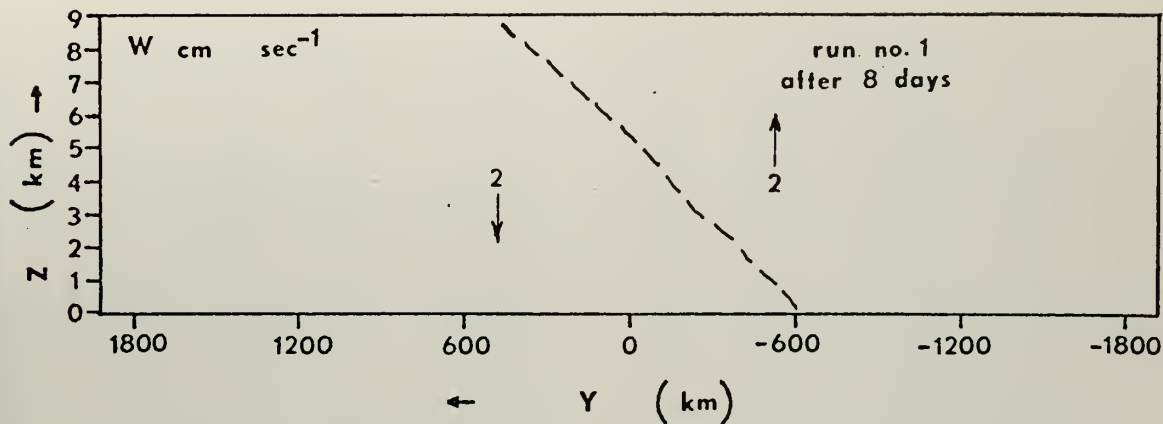


Fig. 1a. Vertical velocity w maxima and the position of the front (---). Run number 1.

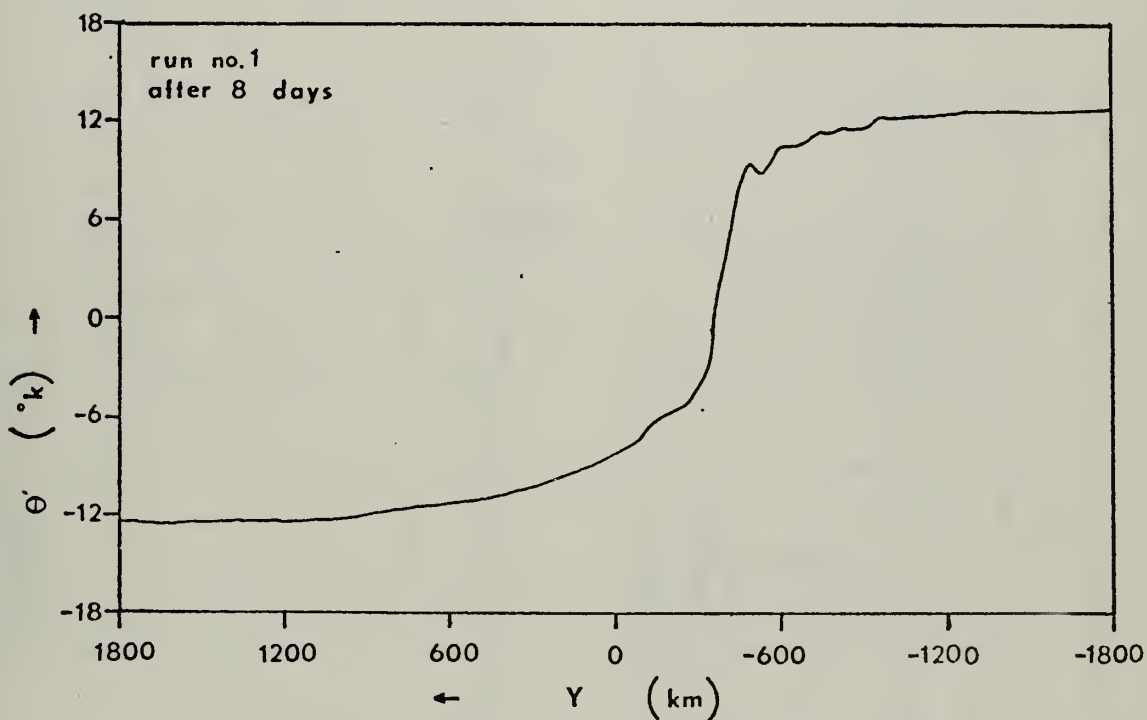


Fig. 1b. Departure potential temperature Θ' at level $z=1.5$ km. Run number 1.

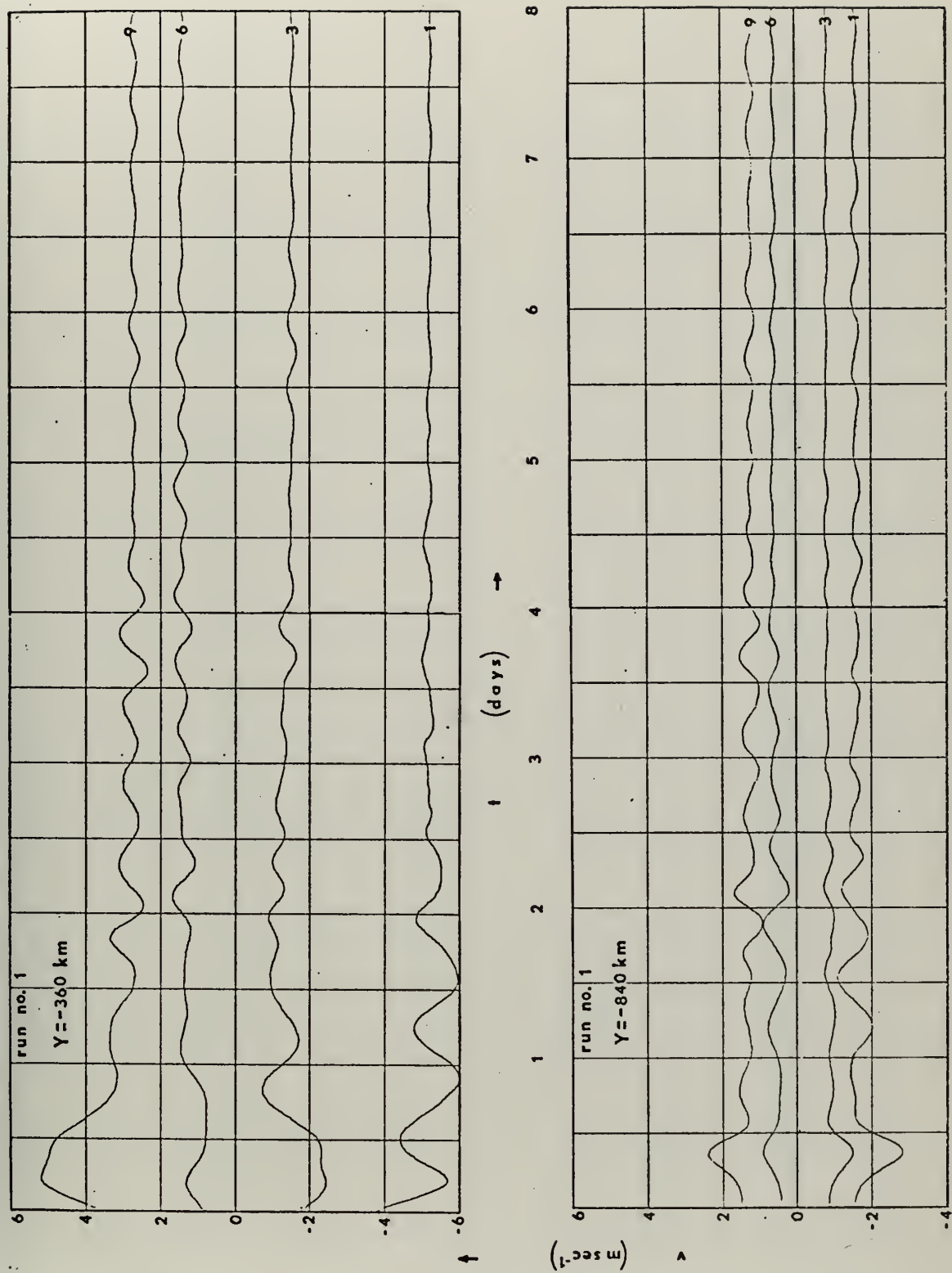


Fig. 2a. Divergent part of the wind v as a function of time at four levels: $z = 0.5$ km (1), $z = 2.5$ km (3), $z = 5.5$ km (6) and $z = 8.5$ km (9) Run number 1.

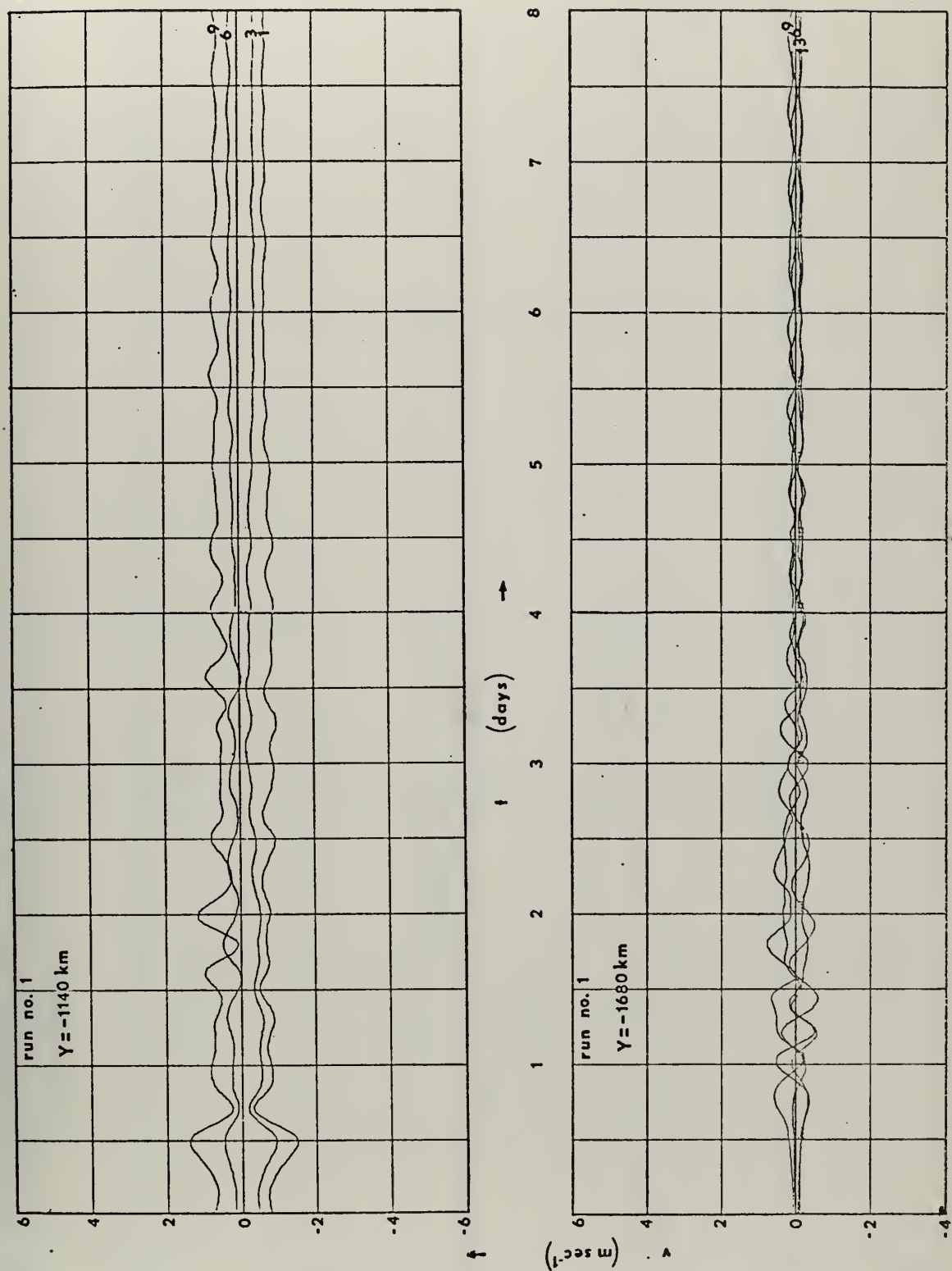


Fig. 2b. Divergent part of the wind v as a function of time at four levels: $z=0.5 \text{ km}$ (1), $z=2.5 \text{ km}$ (3), $z=5.5 \text{ km}$ (6) and $z=8.5 \text{ km}$ (9). Run number 1.

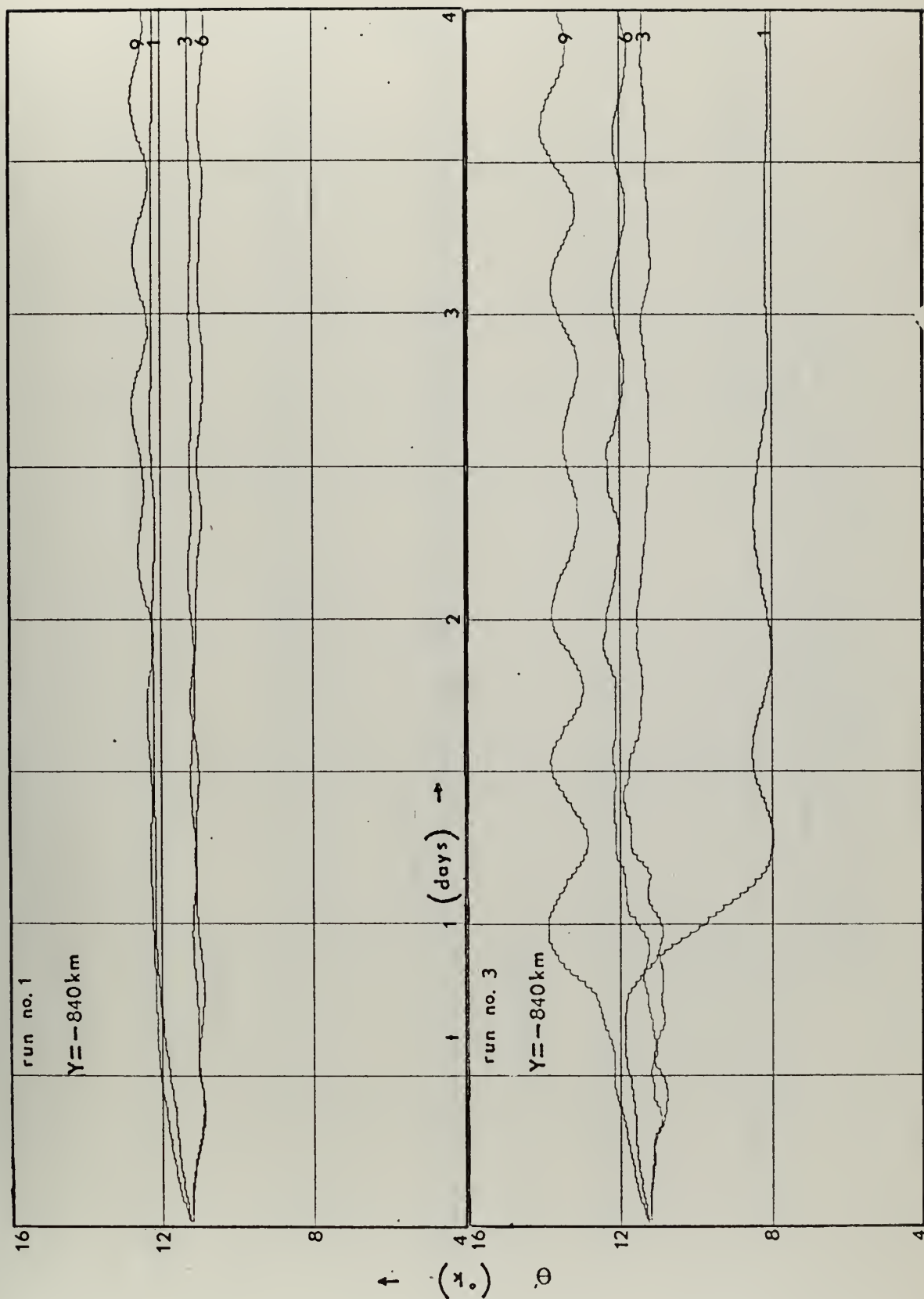


Fig. 3a. Departure potential temperature θ' as a function of time at four levels: $z=0.5$ km (1), $z=2.5$ km (3), $z=5.5$ km (6) and $z=8.5$ km (9). Runs number 1 and 3.

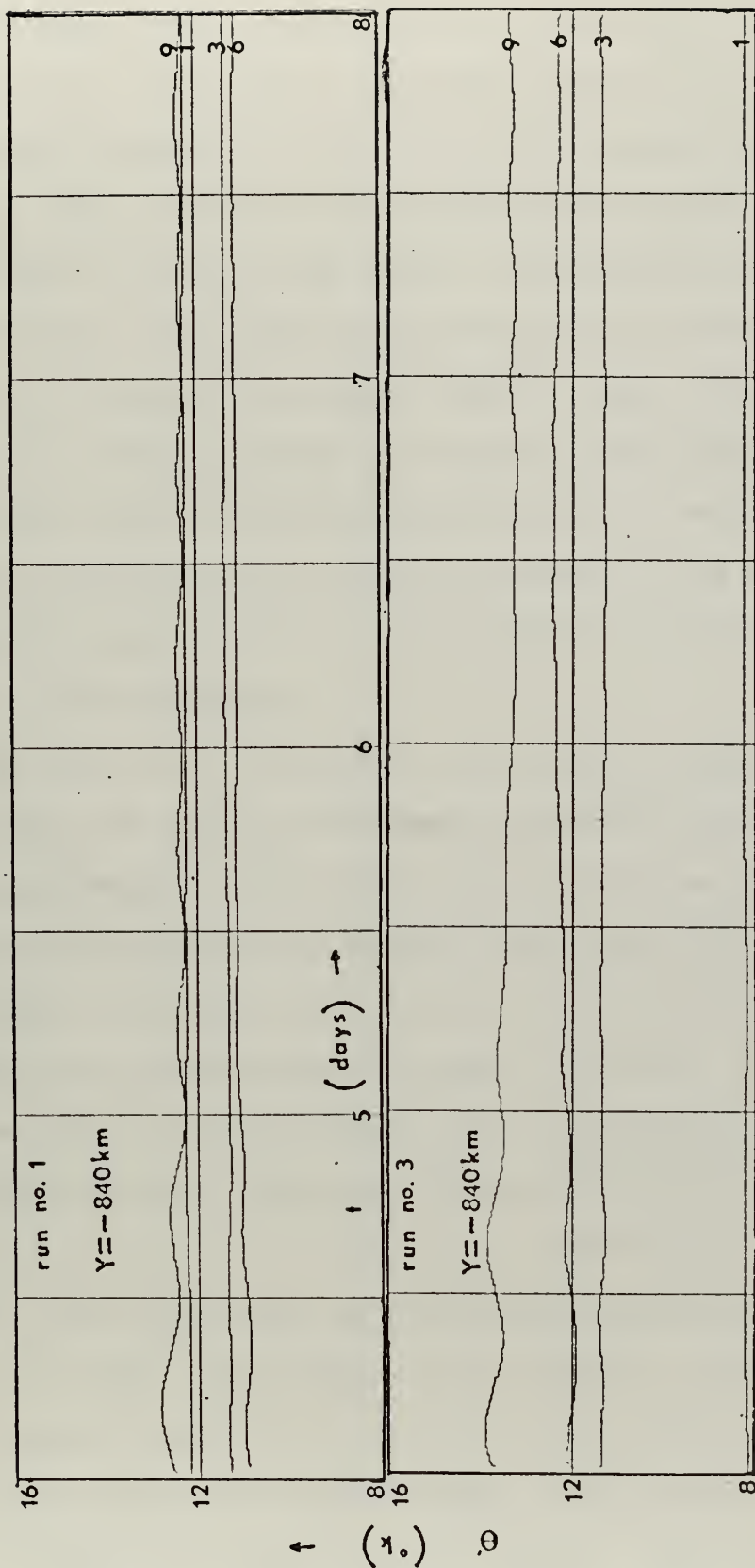


Fig. 3b. Departure potential temperature Θ' as a function of time at four levels: $z=5.5$ km (1), $z=2.5$ km (3) $z=5.5$ km (6) and $z=8.5$ km (9). Runs number 1 and 3.

In run number four, a heating function of $10^{\circ}\text{K day}^{-1}$ is introduced in block form and is 120 km wide, with vertical extent from $z=.5$ km to $z=4.5$ km, and it does not vary with time. This roughly approximated the release of latent heat which would be typical of convective activity in a frontal zone. As can be seen in Fig. 4a and Fig. 4b an increase in vertical velocity and a definite wave pattern in the departure potential temperature θ' ahead of the frontal zone was noted. The gravity waves appeared to be damped as the distance from the frontal zone increased. An additional result of this experiment was that the heating in the warm air greatly strengthened the temperature gradient in the frontal zone. This coincides with the work of Eliassen (1959) concerning the formation of fronts in the atmosphere.

In run number five the heating function took the shape of a sine squared curve with maximum heating occurring in the center of a 300 km wide zone with vertical extent from $z=.5$ km to $z=4.5$ km. This gave a smoother heating function in the frontal zone. The results were similar to run number four except that the vertical velocities and gravity wave amplitudes were reduced slightly, as might be expected.

In run number six the heating function was allowed to vary sinusoidally with time which approximates the build-up and decay of convective activity in the vicinity of a frontal zone. The frequency for a gravity wave with a wave length equal to the scale of the heating zone gave a period of 9.9 hours. As a result of this variation, vertical velocity maxima appeared at $Y \approx \pm 1300$ km which can be seen in Fig. 5a. Other bands of vertical velocity relative maxima appear but only the maximum values are shown in this and subsequent figures. Departure potential temperature fluctuations were also noted at $Y \approx \pm 1300$ km as can be seen

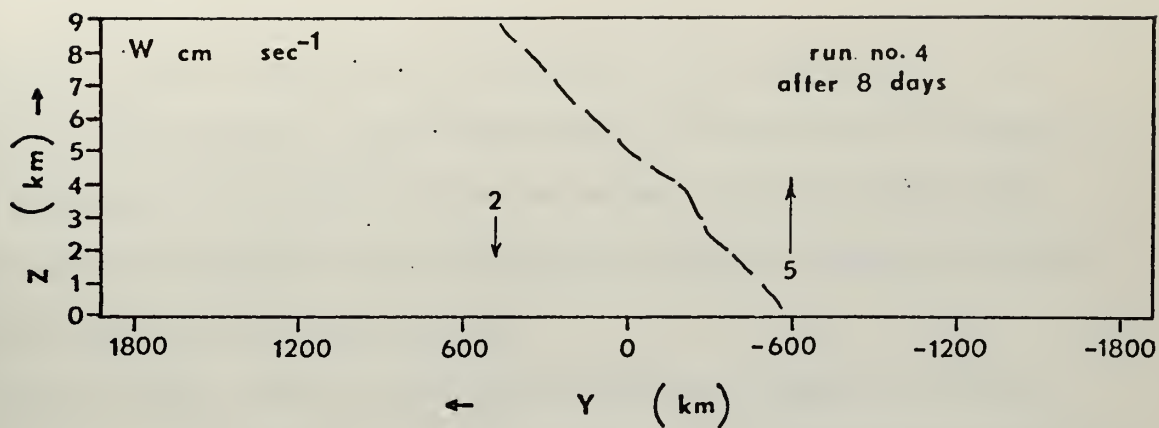


Fig. 4a. Vertical velocity w maxima and the position of the front (---). Run number 4.

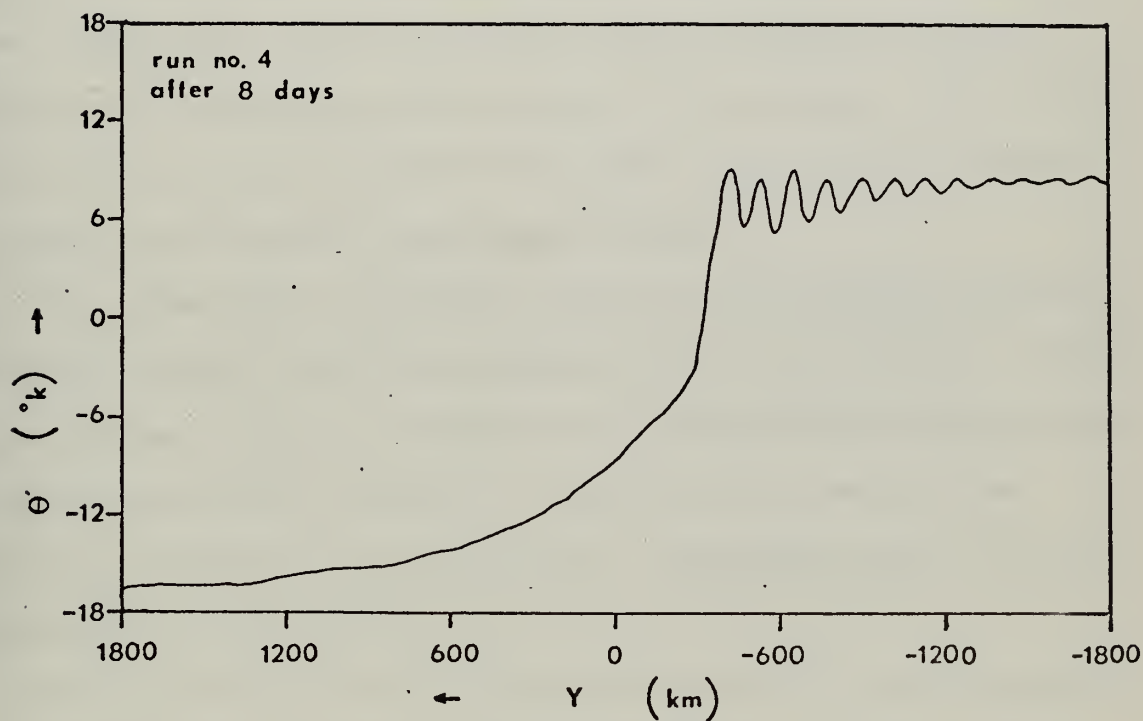


Fig. 4b. Departure potential temperature Θ' at level $z=1.5$ km. Run number 4.

in Fig. 5b. More significantly, the gravity waves generated in the frontal zone propagated in both directions from the front and extend to the boundaries of the model. This can be seen in Fig. 6 which shows definite wave propagation in the departure potential temperature field at various locations on the Y-axis.

In run number seven the heating function was reduced to $3^{\circ}\text{K day}^{-1}$ in order to determine if the patterns found in run number six would still be evident. Gravity wave generation and propagation still occurred but the magnitude of the waves was greatly reduced. Vertical velocity values also decreased and the maximum values returned to the vicinity of the frontal zone. This also was the first run where the heating function was raised and extended from $z=2.5$ km to $z=6.5$ km. This slight modification was made to account for the fact that convective activity in cumulus clouds does not extend to the surface.

In run number eight, the heating function was increased to $30^{\circ}\text{K day}^{-1}$ in order to increase the nonlinear effects in the gravity waves. Vertical velocity maxima remained at $Y \approx \pm 1300$ km but the magnitude of the vertical velocities were greatly increased. Also the first evidence of the formation of standing waves was observed. Well defined bands of vertical motion maxima were also noted.

The heating function was increased to $50^{\circ}\text{K day}^{-1}$ in run number nine and as can be seen in Fig. 7a and Fig. 7b, regions of strong vertical motion were noted throughout the model as well as corresponding variations in potential temperature. Standing long waves appear to form with a wave length of approximately 360 km.

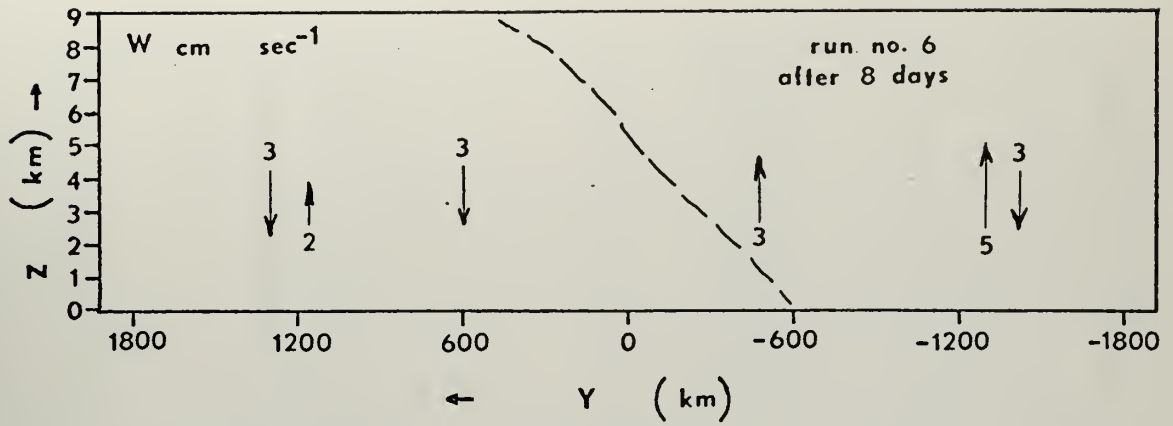


Fig. 5a. Vertical velocity w maxima and the position of the front (---). Run number 6.

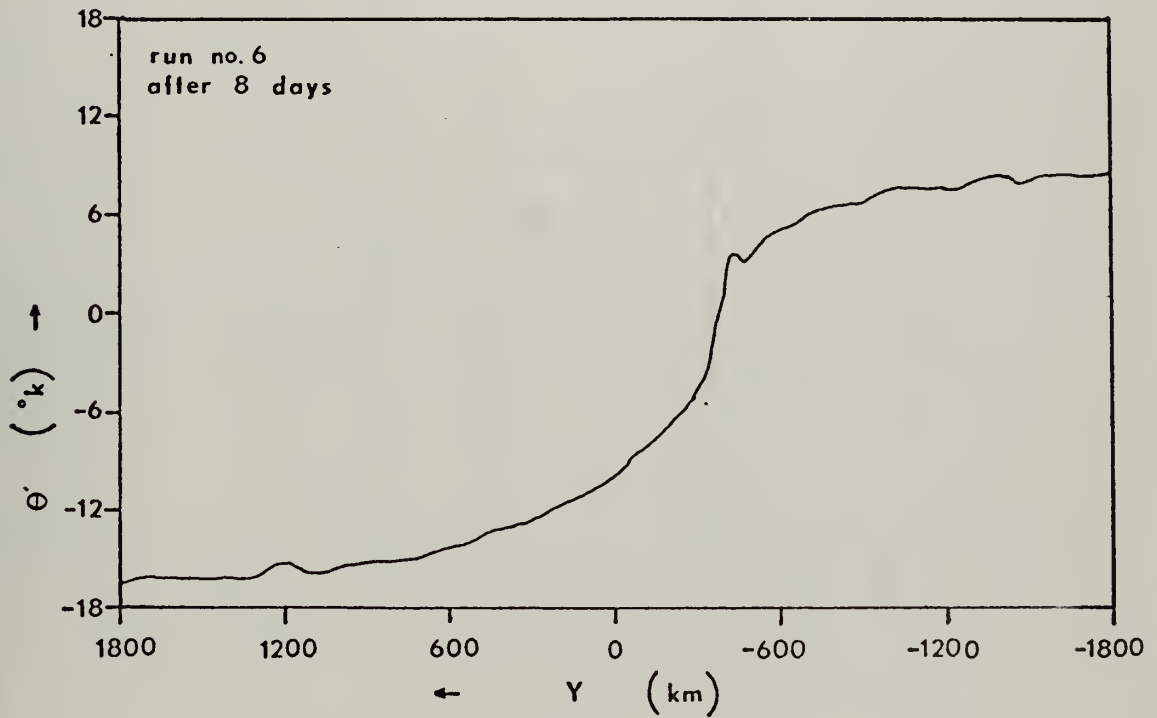


Fig. 5b. Departure potential temperature Θ' at level $z=1.5$ km. Run number 6.

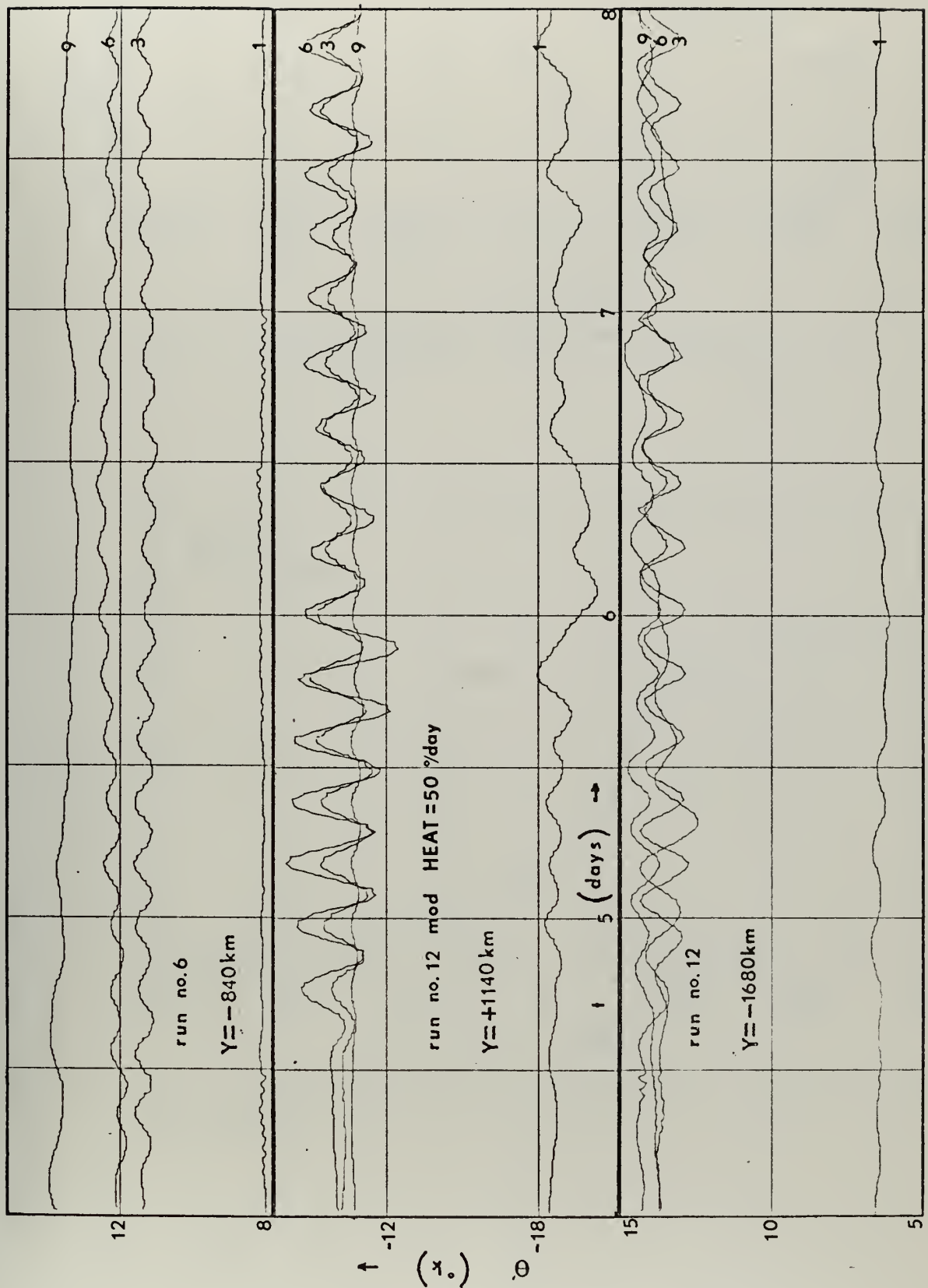


Fig. 6. Departure potential temperature Θ' as a function of time t at four levels: $z = .5 \text{ km}$ (1), $z = 2.5 \text{ km}$ (3), $z = 5.5 \text{ km}$ (6) and $z = 8.5 \text{ km}$ (9). Runs number 6, 12 (mod) and 12.

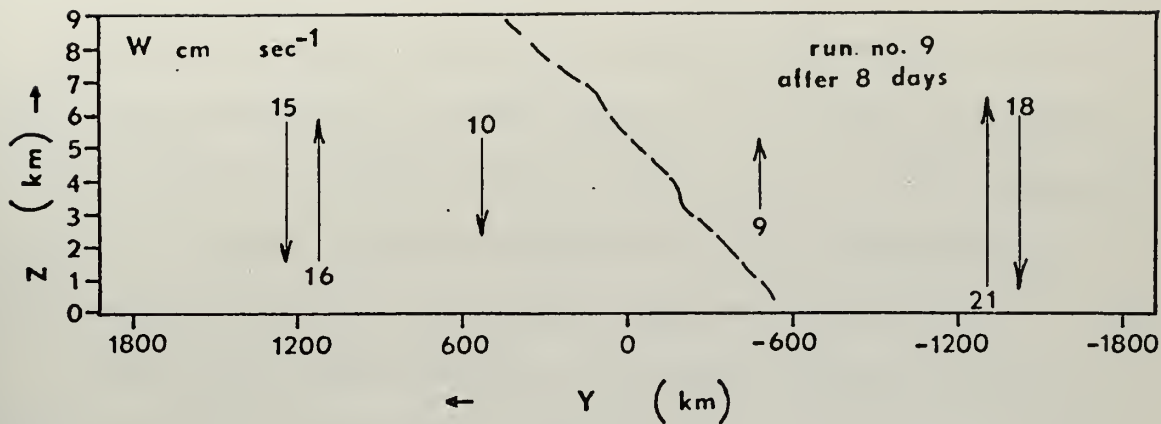


Fig. 7a. Vertical velocity w maxima and the position of the front (---). Run number 9.

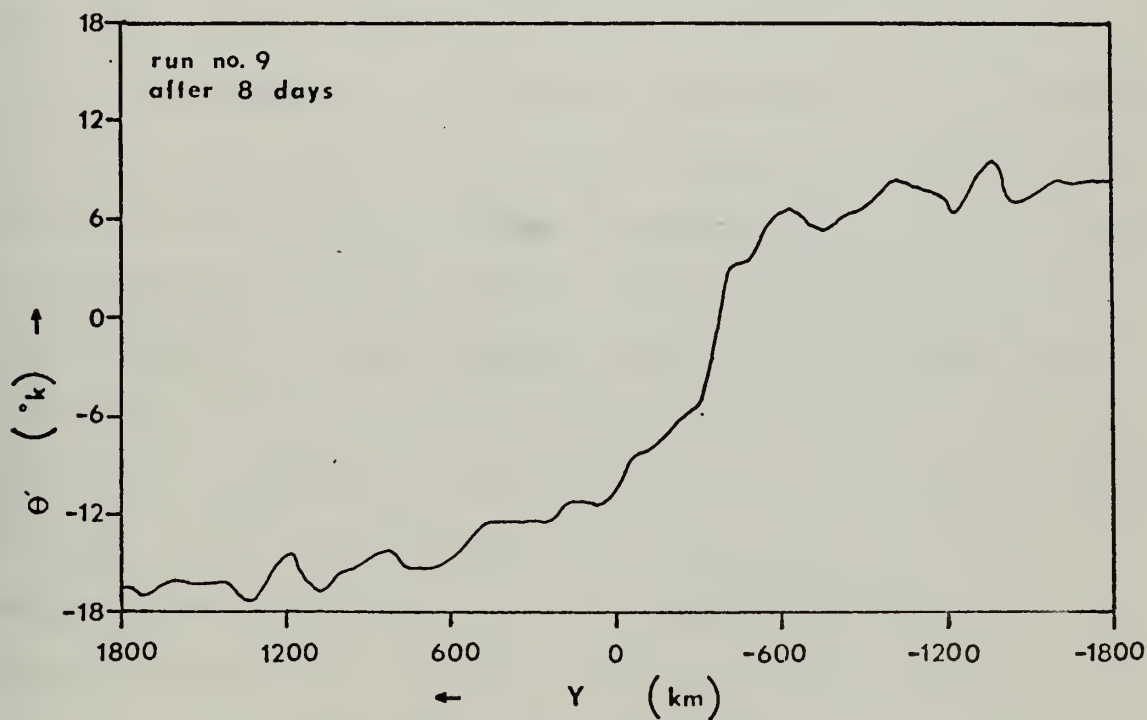


Fig. 7b. Departure potential temperature Θ' at level $z=1.5$ km. Run number 9.

In order to determine what effect a reduction of the horizontal eddy viscosity would have on gravity waves, in run number ten A_m and A_θ were reduced to $7,000 \text{ m}^2 \text{ sec}^{-1}$ from $20,000 \text{ m}^2 \text{ sec}^{-1}$. This reduction appeared to increase vertical velocities and led to standing waves of approximately 130 km, as can be seen in Fig. 8a and Fig. 8b.

In runs eleven through thirteen, the heating function was held at $30^\circ \text{K day}^{-1}$ with A_m and A_θ held at $20,000 \text{ m}^2 \text{ sec}^{-1}$, and the stable layer was altered. In run number eleven the stable layer was removed entirely and the areas of maximum vertical velocities shifted from $Y \approx \pm 1300 \text{ km}$ to $Y \approx \pm 1200 \text{ km}$. In run number twelve a strong stable layer with $\partial \bar{\theta}_1 / \partial z$ equal to $12^\circ \text{K km}^{-1}$ was inserted between $z=1.5 \text{ km}$ and $z=2.5 \text{ km}$. The maximum vertical velocities moved almost to the extremities of the model, away from the frontal zone. Run number thirteen was a repeat of run number two where Tepper's assumptions were tested, but with the inclusion of the heating function. Fig. 9a and Fig. 9b show much the same results as previous experiments with the exception that behind the frontal zone, where no stable layer exists, the maximum w was moved closer to the frontal zone. An interesting result of run number thirteen can be seen in Fig. 10 at $Y=-840 \text{ km}$ and $Y=-1140 \text{ km}$ where a long wave developed at $z=8.5 \text{ km}$ (level nine). This agrees with Alberty and Van Sickle (1969) who found evidence of a mesoscale wave between a frontal zone and a severe storm.

Run number fourteen was another control run which includes all the changes made to the original model. It offers an opportunity to make detailed comparisons with run number one. Table I contains details of parameter changes made between run number one and run number fourteen.

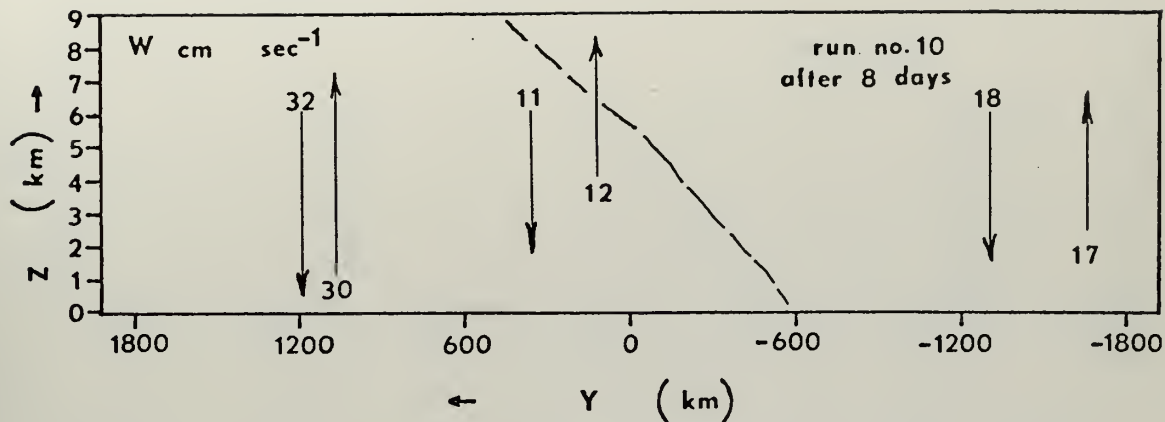


Fig. 8a. Vertical velocity w maxima and the position of the front (---). Run number 10.

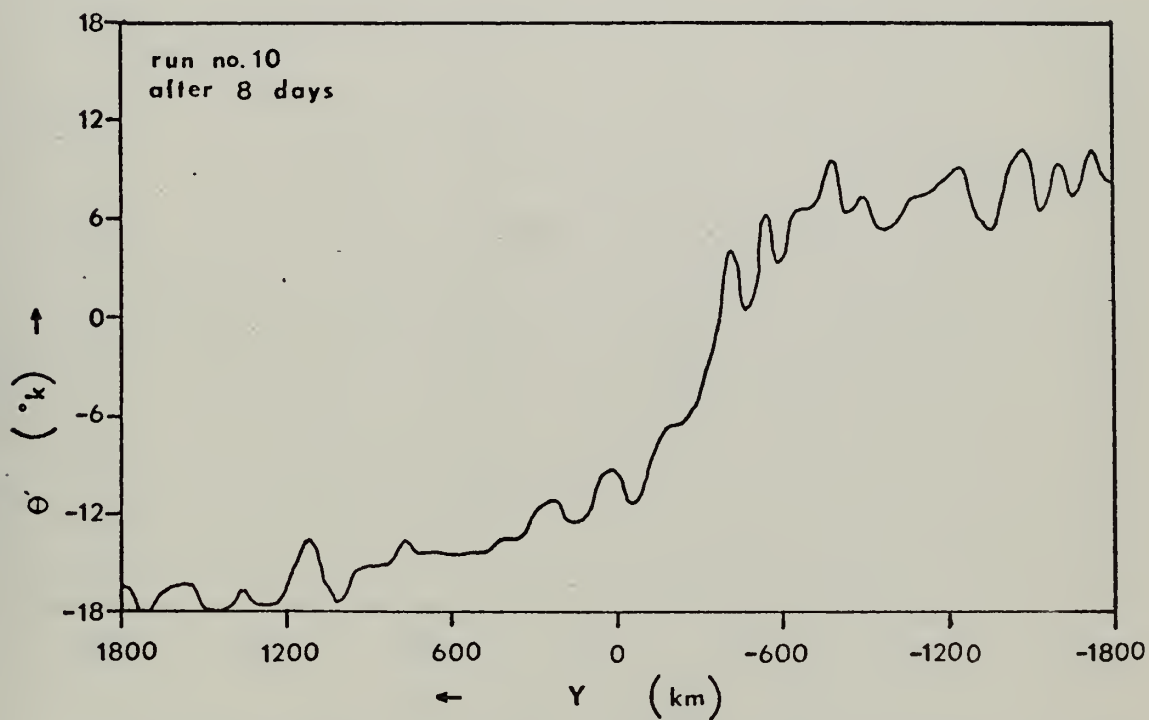


Fig. 8b. Departure potential temperature Θ' at level $z=1.5$ km. Run number 10.

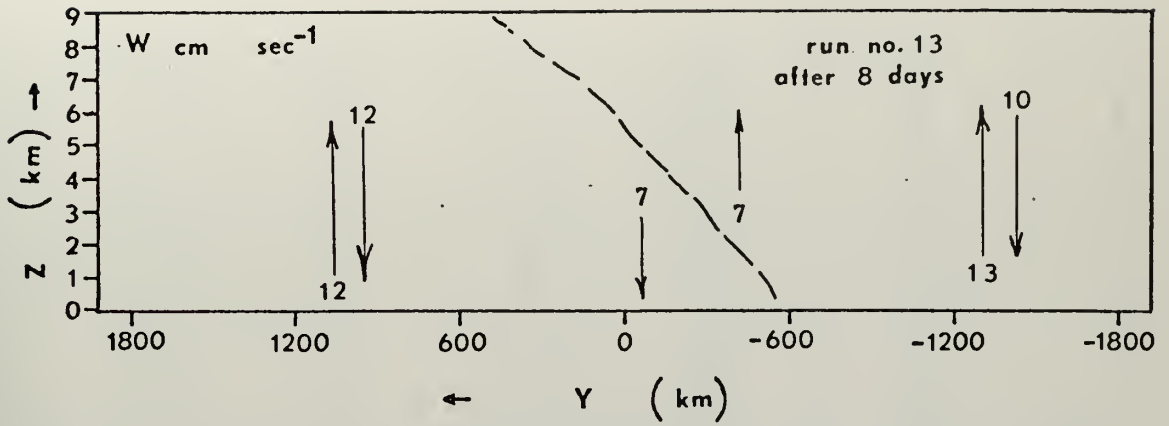


Fig. 9a. Vertical velocity w maxima and the position of the front (---). Run number 13.

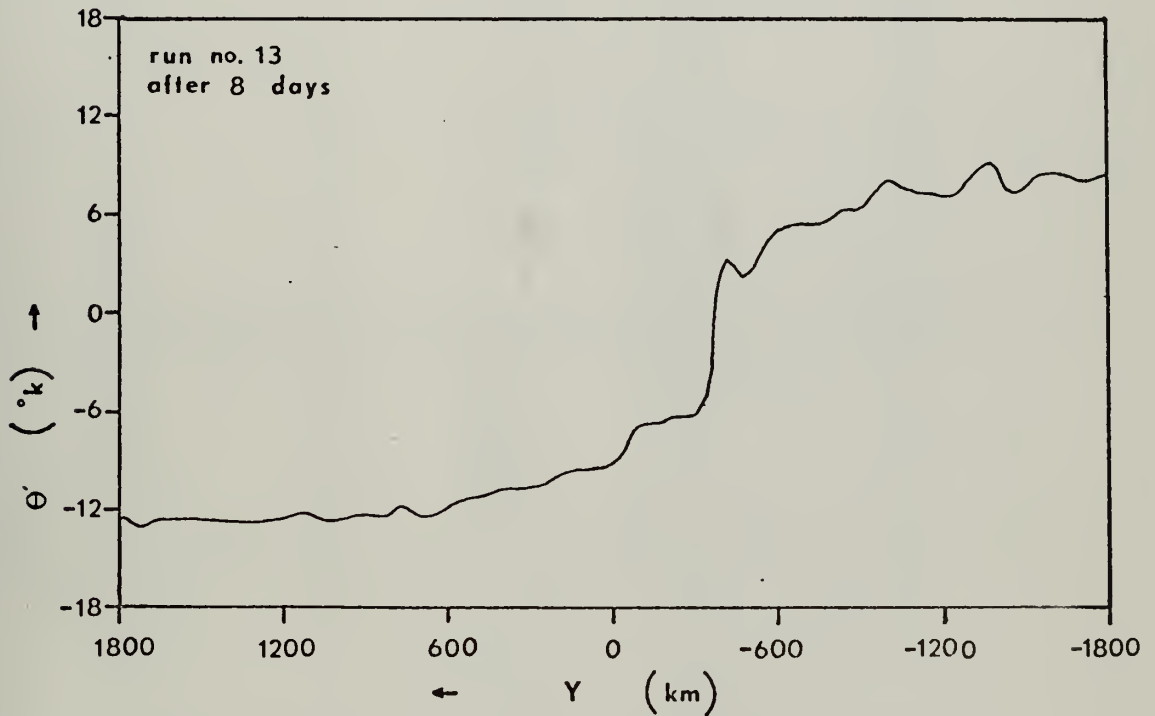


Fig. 9b. Departure potential temperature Θ' at level $z=1.5$ km. Run number 13.

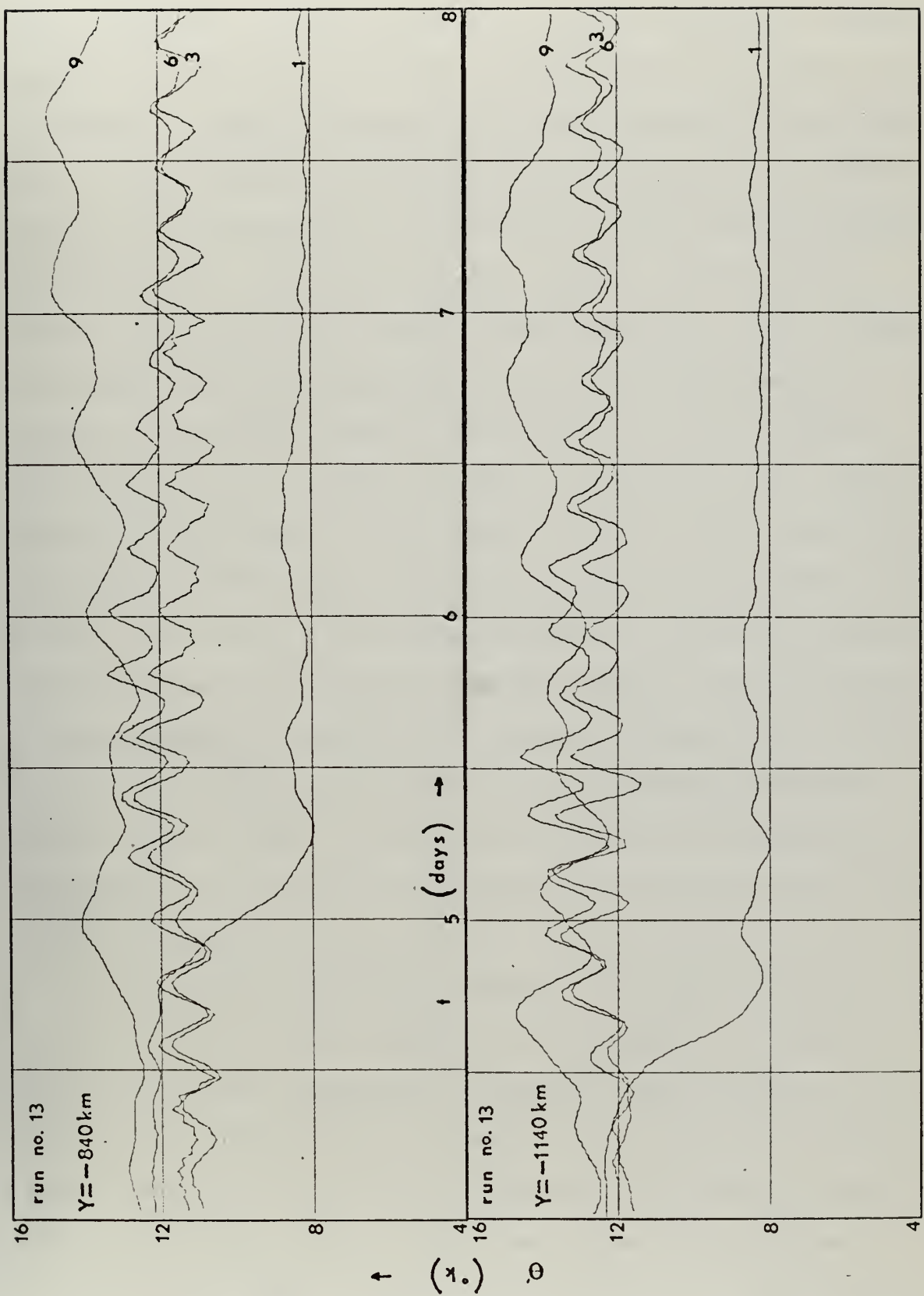


Fig. 10. Departure potential temperature Θ' as a function of time at four levels $z=0.5$ km (1), $z=2.5$ km (3), $z=5.5$ km (6) and $z=8.5$ km (9). Run number 13.

Fig. 11a and Fig. 11b show the now common profile of w and Θ' distributions. Fig. 12a and Fig. 12b show the divergent part of the wind v as a function of time for four positions on the Y-axis ahead of the frontal zone. A phase velocity was obtained from the propagation of the phase lines of the velocity field. In this case the phase speed was approximately 25 m sec^{-1} . This can be compared to Alberty and Van Sickle's mesoscale wave velocity of 14 m sec^{-1} from observed data. Fig. 13 shows an interesting phenomenon which was present in all the cases where gravity waves propagate away from the frontal zone. As the waves at level three (2.5 km) and level six (5.5 km) propagate, the Θ' traces at these two levels diverge. At the point in time where they first begin to diverge, the Θ' trace at level nine (8.5 km) decreases while the Θ' trace at level one (0.5 km) increases slightly. When the Θ' traces at level three and level six begin to converge again, a long wave appears to be generated at level nine, with a marked increase in Θ' . The Θ' traces at $Y = -1140 \text{ km}$ seem to suggest that this divergent/convergent pattern repeats itself. No conclusions will be drawn concerning this phenomenon at this time, but it should be an interesting area for future theory and study.

In runs number 15 and 16 the frequency with which the heating function varies with time is altered. In run number 15 a frequency of $2\pi/52,000$ is used corresponding to a maximum every 14.5 hours. This led to an unrealistic slope in the frontal zone and an outward displacement of maximum w , as can be seen in Fig. 14a. The departure potential temperatures exhibited wide fluctuations as shown in Fig. 14b and Fig. 15. In run number 16 a frequency of $2\pi/20,000$ is used which led to a wave period of 5.5 hours. The results of this experiment were

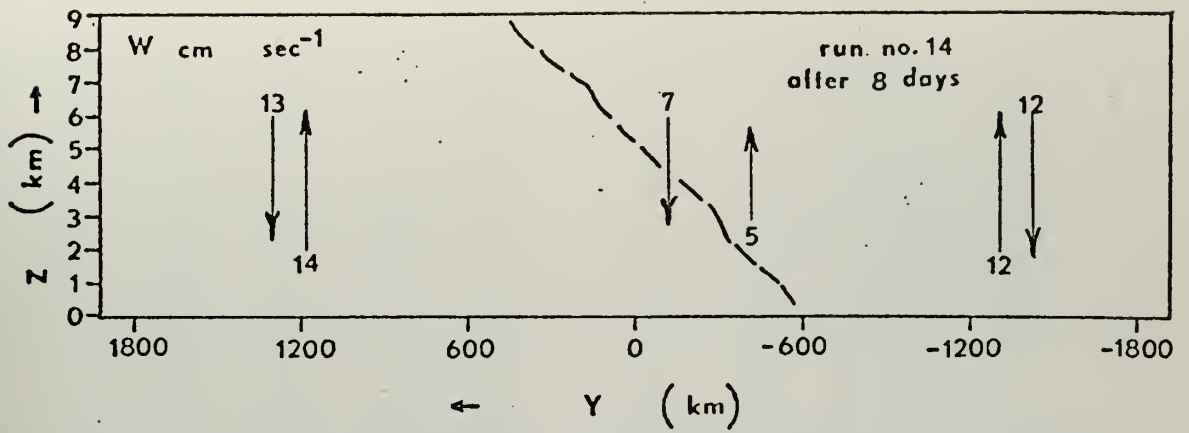


Fig. 11a. Vertical velocity w maxima and the position of the front (---). Run number 14.

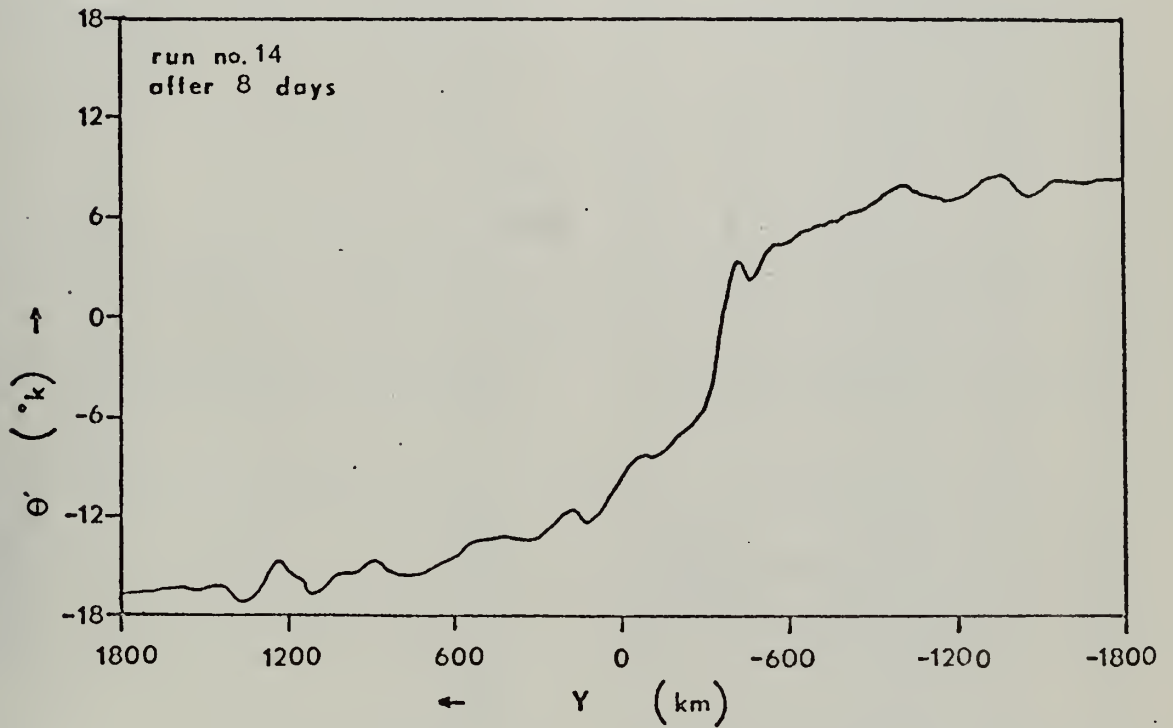


Fig. 11b. Departure potential temperature Θ' at level $z=1.5$ km. Run number 14.

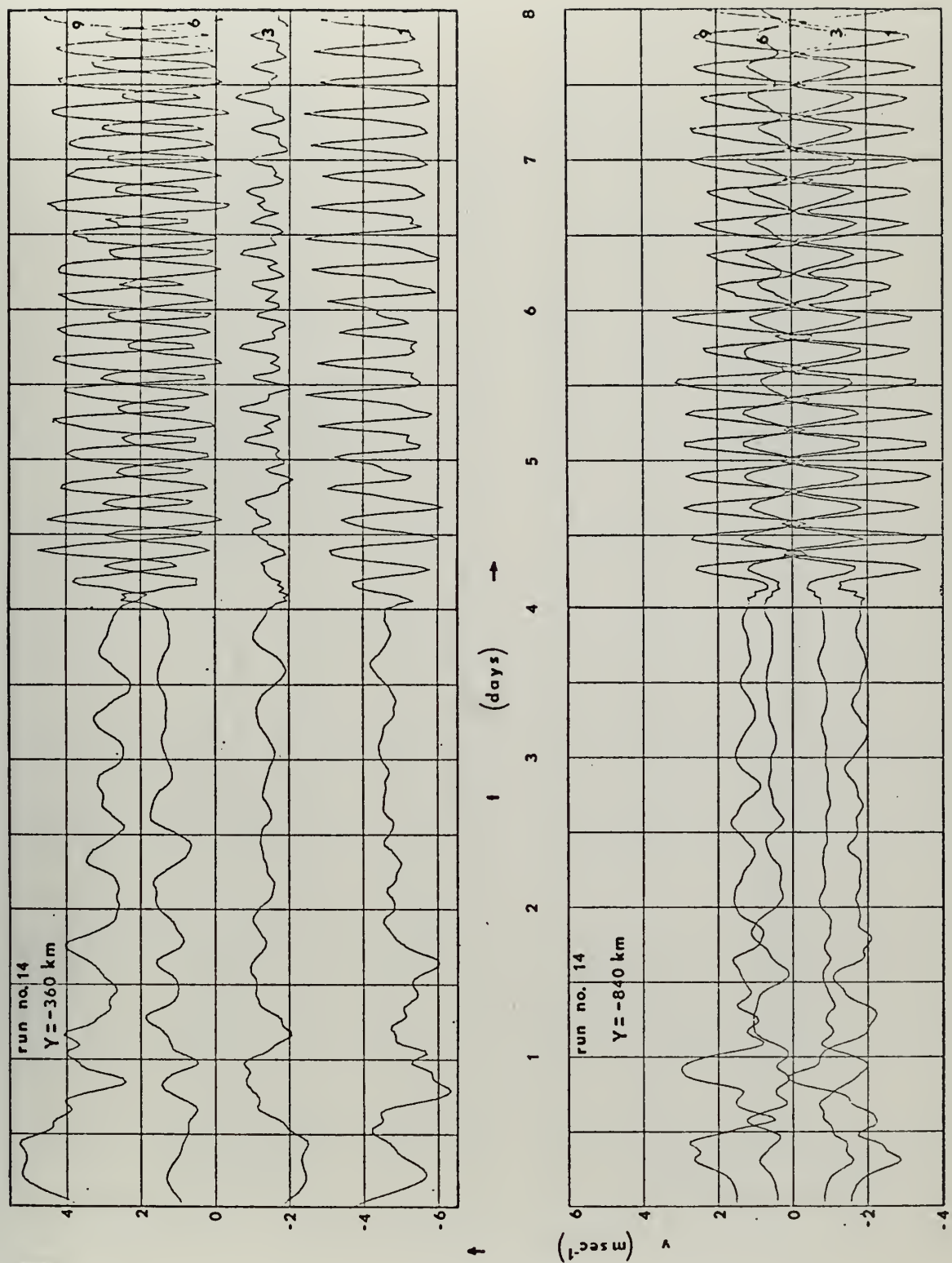


Fig. 12a. Divergent part of the wind v as a function of time at four levels: $z=0.5$ km (1), $z=2.5$ km (3), $z=5.5$ km (6) and $z=8.5$ km (9). Run number 14.

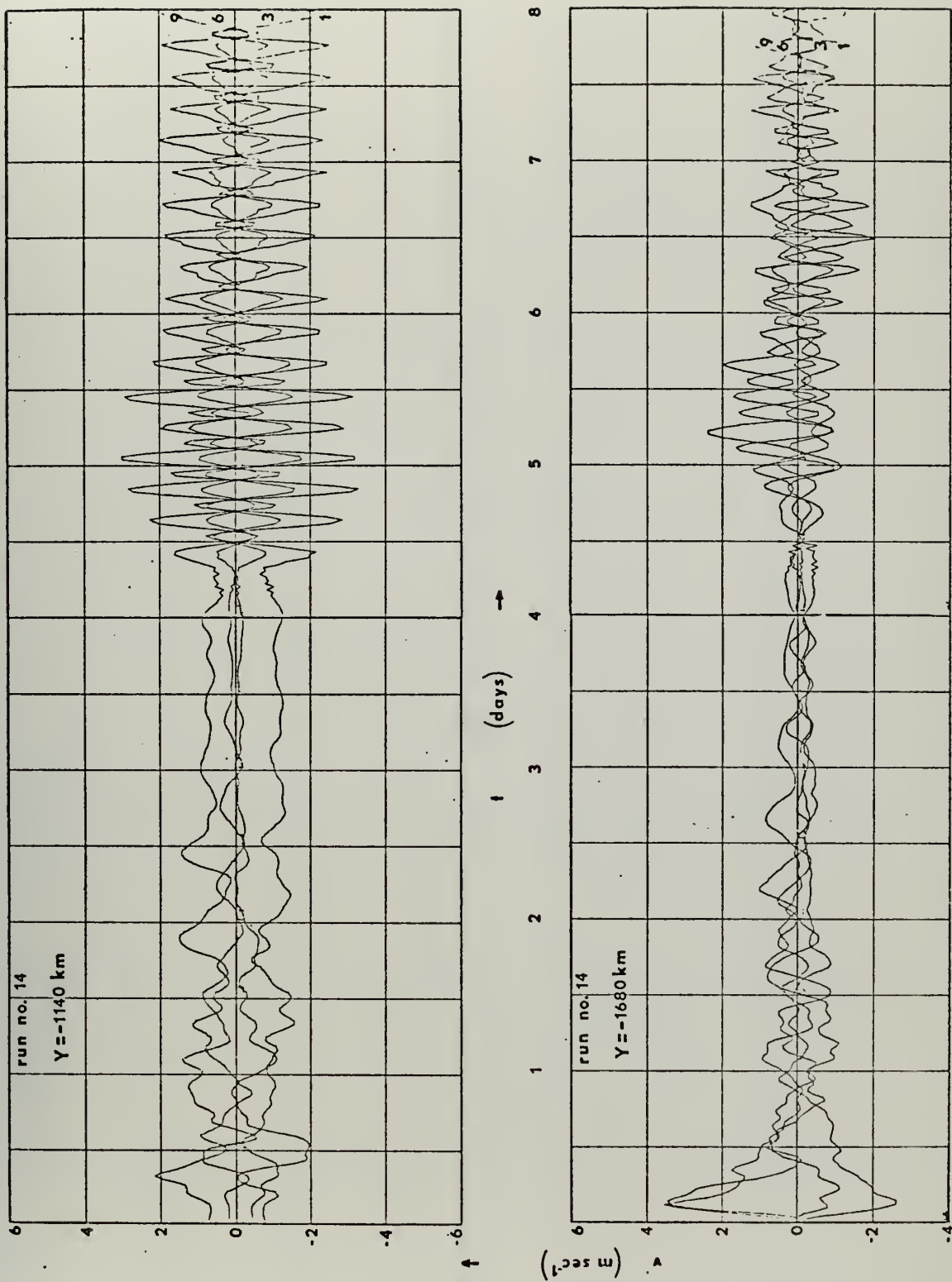


Fig. 12b. Divergent part of the wind v as a function of time at four levels: $z=0.5$ km (1), $z=2.5$ km (3), $z=5.5$ km (6), and $z=8.5$ km (9). Run number 14.

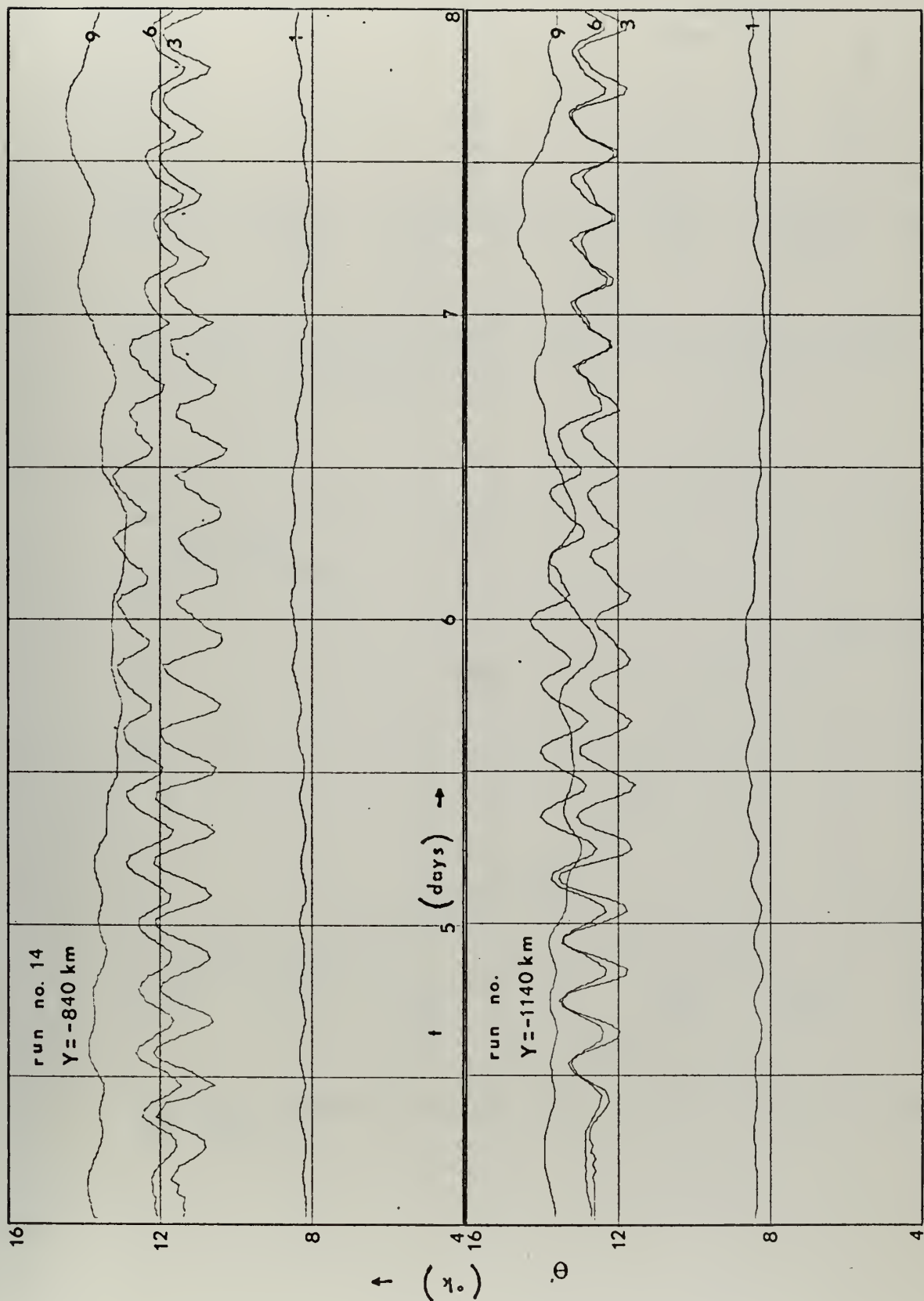


Fig. 13. Departure potential temperature Θ' as a function of time at four levels: $z=0.5$ km (1), $z=2.5$ km (3), $z=5.5$ km (6) and $z=8.5$ km (9). Run number 14.

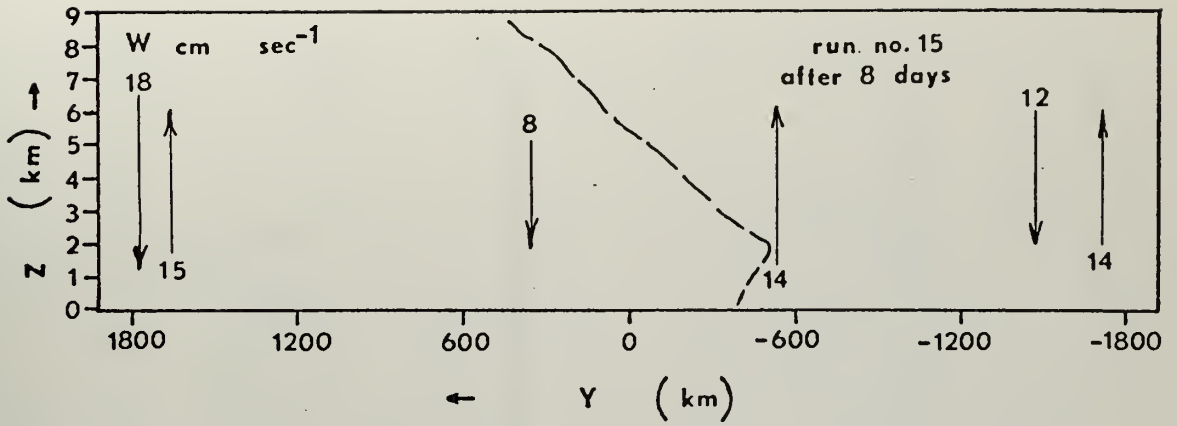


Fig. 14a. Vertical velocity w maxima and the position of the front (---). Run number 15.

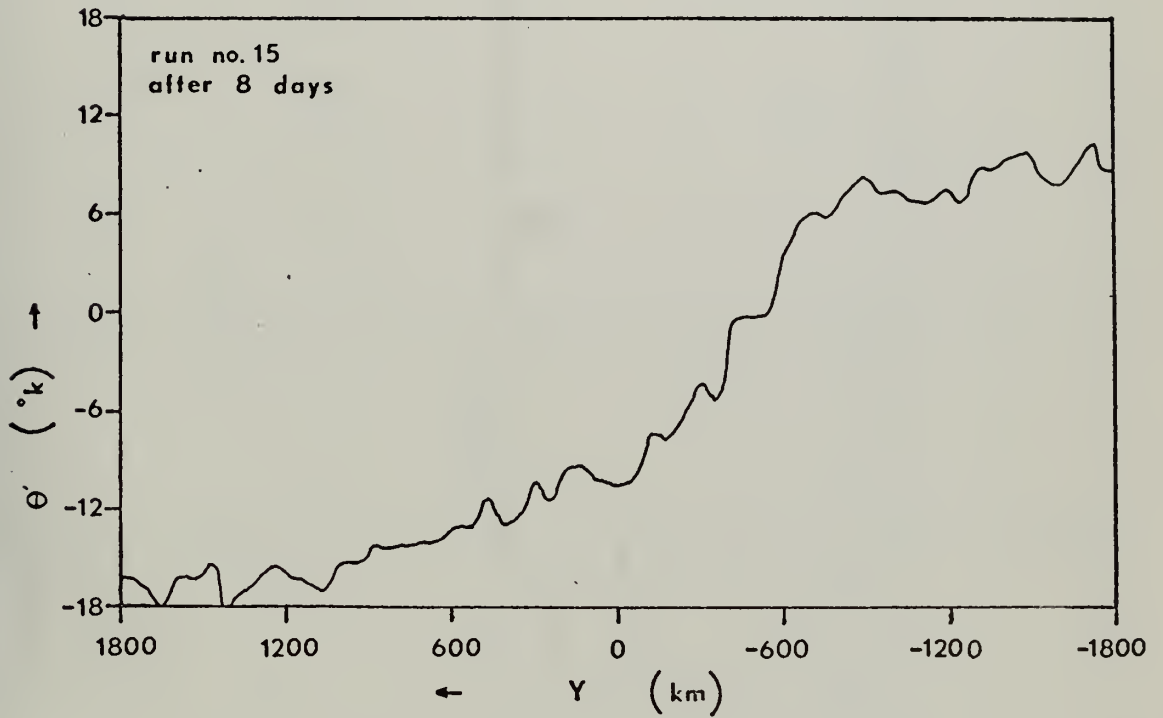


Fig. 14b. Departure potential temperature Θ' at level $z=1.5$ km. Run number 15.

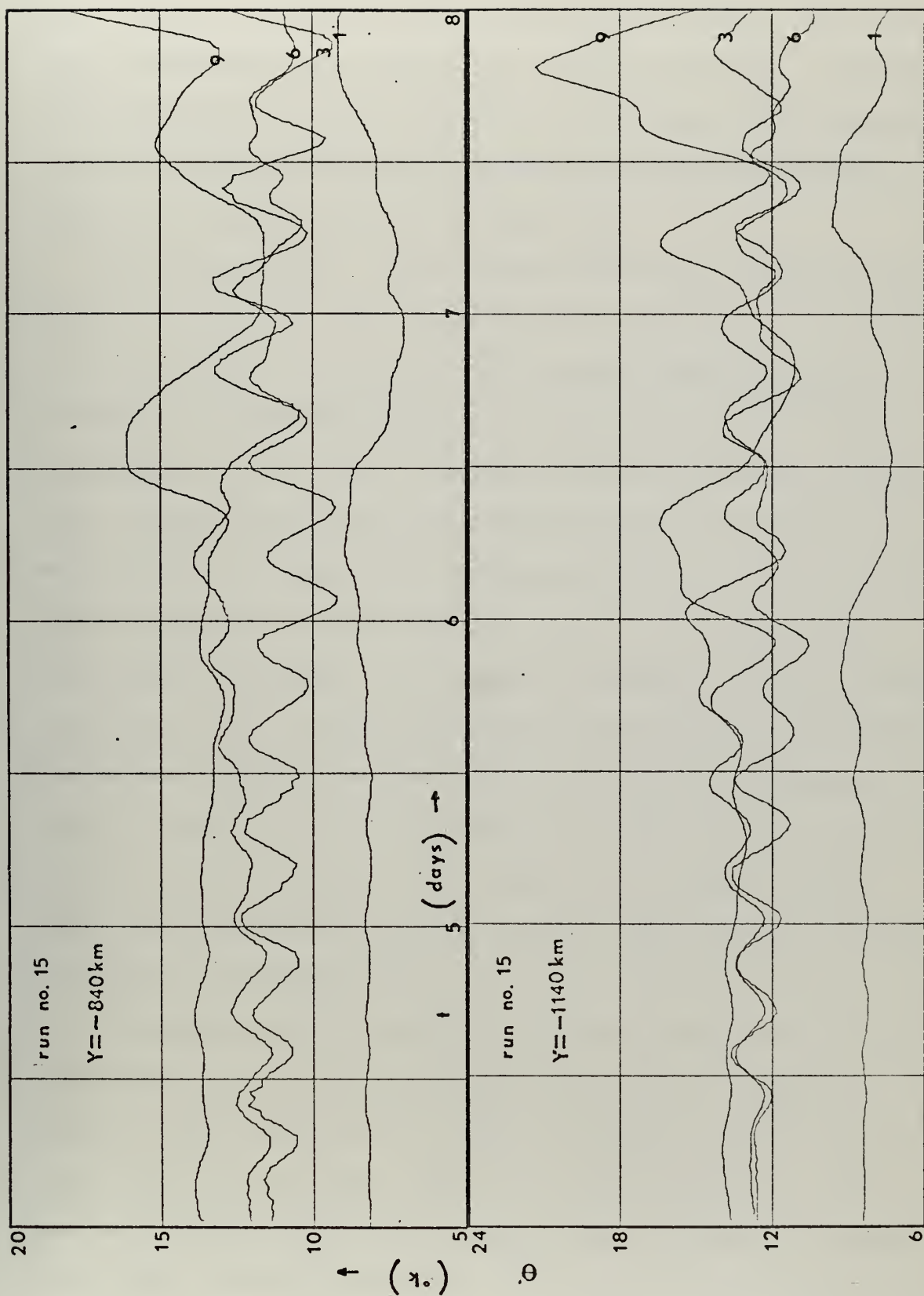


Fig. 15. Departure potential temperature θ' as a function of time at four levels: $z=0.5$ km (1), $z=2.5$ km (3), $z=5.5$ km (6) and $z=8.5$ km (9). Run number 15.

quite similar to the results of run number seven in that gravity waves were generated and did propagate but, even with $C=30^{\circ}\text{K day}^{-1}$ the waves generated were of very small amplitude. The maximum vertical motion was located in the frontal zone and the departure potential temperature profile was similar to that of run number one.

It was expected that if the nonlinear effects were important, that the scale of the waves would become smaller as the waves moved out from the source region. In order to further examine these effects, the boundaries were moved from 1800 km to 2700 km in runs 17-20. These experiments in fact do show a decrease in scale as the waves propagate out. If this decrease comes from nonlinear effects then it should be more pronounced in cases with larger heating. If run 19 with $C=3^{\circ}\text{K day}^{-1}$ is compared to run 20 with $C=100^{\circ}\text{ day}^{-1}$, it can be seen from Table I that the maximum w for run 20 is less than 33 times the maximum w for run 19. If a nonlinear scale reduction occurred in run 20 then the maximum w in that experiment would be larger than the maximum w in run 19, times the ratio of the heating rates. This seems to indicate that the observed scale may not be caused by the nonlinear effects. Rather the observed scale reduction probably comes from the contraction in the basic deformation field.

A comparison was also made with the results obtained by Kurth (1971) who found that in a rotating, continuously stratified atmosphere, hydraulic jumps will form if a certain relationship exists between the Froude number and the Rossby number. The Froude and Rossby numbers were determined for runs seven, nine, fourteen, and twenty, using the Froude number $F=V/[D(g \theta_0^{-1} d \theta_0 / dz)^{1/2}]$, and the Rossby number $R_o = V/fL$, with the result that all four cases fell on the jump side of the

critical curve $F=AR_0^2$, where A is a constant in the range of 6.5-7.5.

Even though jumps should have occurred, it is evident from the previous discussion that they did not occur. The conclusion must be that gravity waves, by themselves, do not cause hydraulic jumps under the conditions of this study.

V. CONCLUSIONS AND RECOMMENDATIONS

The generation of gravity waves in a frontal zone has been investigated numerically. It was determined that the presence of a stable layer ahead of a frontal zone was not sufficient to generate gravity waves or hydraulic jumps. It was found that the addition of a heating function on the face of the front strengthens the frontal zone and generates gravity waves, but that these waves do not propagate away from the frontal zone. It was found that if the heating function applied to the frontal face is allowed to vary sinusoidally with time, that gravity waves will be generated at the front and will propagate in both directions from the frontal zone and induce vertical motion maxima both ahead of and behind the front. It is believed that such motions could cause convective activity and condensation on the less stable warm air side. The amplitude of the gravity waves and the magnitude of the vertical motion maxima varied directly with the heating function and the period of oscillation. A stable layer need not be present for gravity waves to generate and propagate, although the existence and strength of the stable layer appears to affect the distance the vertical velocity maxima are displaced from the front. The vertical velocity maxima fluctuated with the scale of the model but these fluctuations appear to be caused by the contraction in the basic deformation field. The amplitude of the gravity waves generated did not appear to be large enough to induce nonlinear effects which might lead to the formation of hydraulic jumps or squall lines. Squall lines do not appear to be formed by a simple Tepper mechanism but may still be caused by topographic effects.

In future studies using Williams model, a smaller grid scale should be used in order to obtain the fine detail which may be missed using a course grid. The model would be improved if moisture were parameterized or if it were possible to fix the forcing function based on observational data. The latter is not yet possible due to inability to measure the heating distribution. The model should be modified by replacing the rigid plate upper boundary with a boundary which would allow gravity waves to propagate out of the troposphere. It is also suggested that cooling be included both above and below the heating region.

Possibilities for further study using observational data would be to determine if a correlation exists between stable layer strength and displacement of severe storms from a frontal zone, and also whether divergence and convergence of potential temperatures curves between two intermediate levels in the troposphere leads to long wave formation near the tropopause.

LIST OF REFERENCES

1. Albert, R. L., and Van Sickle, K. L., 1969: An analysis of a severe local storm using isentropic trajectories. Technical Report NPS-51AL9081A, Naval Postgraduate School, 135pp.
2. Breeding, R. J., 1972: A nonlinear model of the break-up of internal gravity waves due to their exponential growth with height. J. Geophys. Res., 77, 2681-2692.
3. Eliassen, A., 1959: On the formation of fronts in the atmosphere. The Atmosphere and the Sea in Motion, New York, Rockefeller Institute Press and Oxford University Press, 277-287.
4. Fujita, and Bohan, 1967: Detailed views of mesoscale cloud patterns filmed from ATS-1 pictures, January 7 and 8, 1967. Film.
5. Gossard, E. E., 1962: Vertical flux of energy in the lower ionosphere from internal gravity waves generated in the troposphere. J. Geophys. Res., 67, 745-757.
6. _____, Jensen, D. R., and Richter, J. H., 1971: An analytical study of tropospheric structure as seen by high-resolution radar. J. Atmos. Sci., 28, 794-807.
7. Hines, C. O., 1960: Internal atmospheric gravity waves at ionospheric heights. Can. J. Phys., 38, 1441-1481.
8. Kurth, R. P., 1971: The formation of hydraulic jumps in a rotating, continuously stratified system. Masters thesis, Naval Postgraduate School, 39pp.
9. Ogura, Y., and Charney, J. G., 1962: A numerical model of thermal convection in the atmosphere. Proc. Int. Symp. on Numer. Weather Predict., Tokyo, 431-452.
10. Platzman, G. W., 1954: The computational stability of boundary conditions in numerical integration of the velocity equation. Arch. Meteor. Geophys. Bioklim., 7, 29-40.
11. Sasaki, Y., 1959: A numerical experiment for squall-line formation. J. Meteor., 16, 347-353.
12. Tepper, J., 1952: The application of the hydraulic analogy to certain atmospheric flow problems. Weather Bur. Res. Pap. 35, 50 pp., U. S. Government Printing Office, Washington, D. C.
13. Williams, R. T., 1967: Atmospheric frontogenesis: A numerical experiment. J. Atmos. Sci., 24, 627-641.
14. _____, 1972a: Quasi-geostrophic versus non-geostrophic frontogenesis. J. Atmos. Sci., 29, 3-10.
15. _____, 1972b: Steady-state fronts. Unpublished manuscript.

INITIAL DISTRIBUTION LIST

| | No. Copies |
|---|------------|
| 1. Defense Documentation Center Cameron Station Alexandria, Virginia 22314 | 2 |
| 2. Library, Code 0212 Naval Postgraduate School Monterey, California 93940 | 2 |
| 3. Department of Meteorology Naval Postgraduate School Monterey, California 93940 | 3 |
| 4. Department of Oceanography Naval Postgraduate School Monterey, California 93940 | 1 |
| 5. National Center for Atmospheric Research Box 1470 Boulder, Colorado 80302 | 1 |
| 6. National Severe Storms Laboratory 1616 Halley Avenue Norman, Oklahoma 73069 | 1 |
| 7. Dr. Joanne Simpson Experimental Meteorology Laboratory National Oceanographic and Atmospheric Administration Coral Gables, Florida 33124 | 1 |
| 8. Dr. Y. Sasaki Department of Meteorology University of Oklahoma Norman, Oklahoma 73069 | 1 |
| 9. Dr. N. A. Phillips 54-1422 M. I. T. Cambridge, Massachusetts 02139 | 1 |
| 10. Dr. M. G. Wurtele Department of Meteorology UCLA Los Angeles, California 90024 | 1 |
| 11. Dr. D. D. Houghton Department of Meteorology University of Wisconsin Madison, Wisconsin 53706 | 1 |

12. Dr. Jerry D. Mahlman 1
Geophysical Fluid Dynamics Laboratory/NOAA
Princeton University
P. O. Box 308
Princeton, New Jersey 08540
13. Professor Noel E. Boston 1
Department of Oceanography
Naval Postgraduate School
Monterey, California 93940
14. Professor Jerry L. Galt 1
Department of Oceanography
Naval Postgraduate School
Monterey, California 93940
15. Professor Ronnie L. Alberty 1
Department of Meteorology
Naval Postgraduate School
Monterey, California 93940
16. Professor Russell Elsberry 1
Department of Meteorology
Naval Postgraduate School
Monterey, California 93940
17. Dr. George J. Haltiner 1
Department of Meteorology
Naval Postgraduate School
Monterey, California 93940
18. Dr. Roger Terry Williams 10
Department of Meteorology
Naval Postgraduate School
Monterey, California 93940
19. LCDR Robert O. Given 5
COMNAVFORKOREA
APO, San Francisco 96301
20. Dr. R. L. Haney 2
Department of Meteorology
Naval Postgraduate School
Monterey, California 93940
21. Professor Tetsuya Fujita 1
Department of Geophysical Sciences
University of Chicago
Chicago, Illinois 60637
22. Dr. John Young 1
Department of Meteorology
University of Wisconsin
Madison, Wisconsin 53706

- | | |
|-------------------------------------|---|
| 23. Dr. Earl Gossard | 1 |
| Environmental Research Laboratory | |
| WPL | |
| NOAA | |
| Boulder, Colorado 80302 | |
| 24. Professor Y. Ogura | 1 |
| Laboratory for Atmospheric Research | |
| University of Illinois | |
| Urbana, Illinois 61801 | |
| 25. Dr. John Lewis | 1 |
| Laboratory for Atmospheric Research | |
| University of Illinois | |
| Urbana, Illinois 61801 | |

Unclassified

Security Classification

DOCUMENT CONTROL DATA - R & D

(Security classification of title, body of abstract and indexing annotation must be entered when the overall report is classified)

ORIGINATING ACTIVITY (Corporate author)

Naval Postgraduate School
Monterey, California 93940

2a. REPORT SECURITY CLASSIFICATION

Unclassified

2b. GROUP

REPORT TITLE

Numerical Simulation of the Generation of Gravity Waves in a Frontal Zone

DESCRIPTIVE NOTES (Type of report and, inclusive dates)

Master's Thesis; September 1972

AUTHOR(S) (First name, middle initial, last name)

Robert Ole Given

REPORT DATE

September 1972

7a. TOTAL NO. OF PAGES

7b. NO. OF REFS

a. CONTRACT OR GRANT NO.

9a. ORIGINATOR'S REPORT NUMBER(S)

b. PROJECT NO.

c.

9b. OTHER REPORT NO(S) (Any other numbers that may be assigned this report)

d.

0. DISTRIBUTION STATEMENT

Approved for public release; distribution unlimited.

1. SUPPLEMENTARY NOTES

12. SPONSORING MILITARY ACTIVITY

Naval Postgraduate School
Monterey, California 93940

3. ABSTRACT

The generation of gravity waves in a frontal zone is investigated with a numerical model. The solutions show that gravity waves can be generated in a frontal zone by the application of a heating function which varies sinusoidally with time, and that such waves propagate both ahead of and behind the frontal zone. The amplitude of the waves are directly proportional to the magnitude of the forcing function and to the period of sinusoidal oscillation. Even with large heating rates, no hydraulic jumps are formed.

14.

KEY WORDS

LINK A

LINK B

LINK C

ROLE

WT

ROLE

WT

ROLE

WT

Frontal zone
Gravity waves
Hydraulic jumps
Severe storms
Squall lines

Thesis

138185

G4563 Given

c.1

Numerical simulation
of the generation of
gravity waves in a
frontal zone.

Thesis

138185

G4563 Given

c.1

Numerical simulation
of the generation of
gravity waves in a
frontal zone.

thesG4563

Numerical simulation of the generation o



3 2768 002 02927 4

DUDLEY KNOX LIBRARY